



Localized geochemical variability produced by depositional and diagenetic processes in a 2.8 Ga Ca-carbonate system: A cautionary paradigm

Philip Fralick^{a,*}, Tobias Himmler^b, Stefan V. Lalonde^c, Robert Riding^d

^a Department of Geology, Lakehead University, Thunder Bay, Ontario, Canada

^b MARUM – Center for Marine Environmental Sciences and Faculty of Geosciences, University of Bremen, 28359 Bremen, Germany

^c Laboratoire Geo-Océan, Institut Universitaire Européen de la Mer, Université de Bretagne Occidentale, 29280 Plouzané, France

^d Department of Earth, Environmental and Planetary Sciences, University of Tennessee, Knoxville, TN 37996, USA

ARTICLE INFO

Keywords:

Steep rock
Archean carbonate
Diagenesis
Rare earth elements
Ocean chemistry
Element mobility

ABSTRACT

A plethora of proxies has been developed over the preceding two decades in attempts to investigate the geochemistry of the Archean ocean–atmosphere system, and in particular oxygen levels. Unfortunately the necessary parallel investigations of the effects that localized ocean chemistry and diagenesis can have on Archean sediments have commonly not kept pace. We used micro-analytical techniques (LA-ICP-MS and XRF scanning), to distinguish the effects of changes in water composition during precipitation and diagenesis on marine limestone precipitates at the margin and interior of a 2.8 Ga carbonate platform (Mosher Carbonate, Steep Rock Group) in western Superior Province, Canada. Platform margin meter-scale hybrid giant domes consist of centimetric interlayered couplets of (1) Sr-rich crystal fan fabric and cusped fenestral microbialite, both with pronounced negative Ce-anomalies, and (2) net-like fenestral microbialite, rich in diagenetic cement with diminished concentrations of Sr and lacking negative Ce anomalies. The elevated Sr in the crystal fan fabric and cusped fenestral microbialite is a general sign of less diagenetic alteration, as is preservation of millimeter-scale chemical differences. XRF mapping revealed that samples that otherwise appear pristine from a second site on the platform rim, near a zone of alteration in the limestone, have ferroan dolomite-filled micro-fractures with Mn flooding of the surrounding calcite and lack Ce anomalies. Platform interior silicified and ferroan dolomitized columnar stromatolites have some calcite laminae, but exceptionally low Sr contents indicate that they formed by dedolomitization. In several horizons REE patterns identical to those of offshore iron formation, replacement of calcite by iron carbonate, and the presence of iron oxides all suggest that short term flooding of the platform by offshore seawater episodically introduced ferroan dolomitizing fluids. Overall, these data indicate a restricted marine environment subject to periodic flooding by offshore waters that caused seafloor diagenetic alteration and precipitation of iron hydroxides. In this system the least altered limestone was the lithotype most likely to retain evidence of free oxygen. Samples with abundant phreatic cement and/or Mn alteration associated with micro-fractures were liable to have experienced REE mobilization. Detailed studies that integrate both depositional and diagenetic information are critical for the correct interpretation of geochemical data from sedimentary rocks.

1. Introduction

The use of elemental and isotopic proxies in marine sedimentary rocks to interpret the large-scale geochemistry of the atmosphere-hydrosphere system has greatly expanded over the past twenty years. This approach is based on the premise that the fluid from which the proxy was deposited was seawater with an average oceanic composition, and that the proxy has not been subsequently altered by another fluid.

This in turn implies that the mineral(s) containing the proxy has/have remained non-reactive, thereby providing a secure home for the proxy. In addition, the sediment must have been initially deposited in an area of the ocean not affected by freshwater influx, and not sufficiently isolated from the main world ocean to have atypical seawater chemistry. It must also be assumed that there were no element/isotopic concentration gradients with depositional depth that would have affected the proxy of interest. These are stringent requirements. In the case of Precambrian

* Corresponding author.

E-mail addresses: philip.fralick@lakeheadu.ca (P. Fralick), thimmler@uni-bremen.de (T. Himmler), stefan.lalonde@univ-brest.fr (S.V. Lalonde), rriding@utk.edu (R. Riding).

<https://doi.org/10.1016/j.precamres.2024.107499>

Received 10 December 2023; Received in revised form 26 June 2024; Accepted 28 June 2024

Available online 4 July 2024

0301-9268/© 2024 The Authors. Published by Elsevier B.V. This is an open access article under the CC BY-NC-ND license (<http://creativecommons.org/licenses/by-nc-nd/4.0/>).

atmospheric oxygen levels, it is not always clear that studies consider the possibility that the proxy being used may not be representative of average ocean water and/or that it has not been altered by subsequent interchange with another fluid.

In addition carbonate rocks are particularly susceptible to geochemical changes arising from syn- and post-depositional processes. For example, due to their shallow depth, platform sediments in photic

zone surface waters were susceptible to extensive modification during falling stage to lowstand systems tract development. In addition, the interiors of rimmed platforms can be partially to fully isolated from the ocean, and develop hyper-saline or brackish water depending on the climate. In these conditions, precipitation without significant seawater recharge can progressively modify platform interior water chemistry. Conversely prolonged rainfall and influx of fresh water into isolated

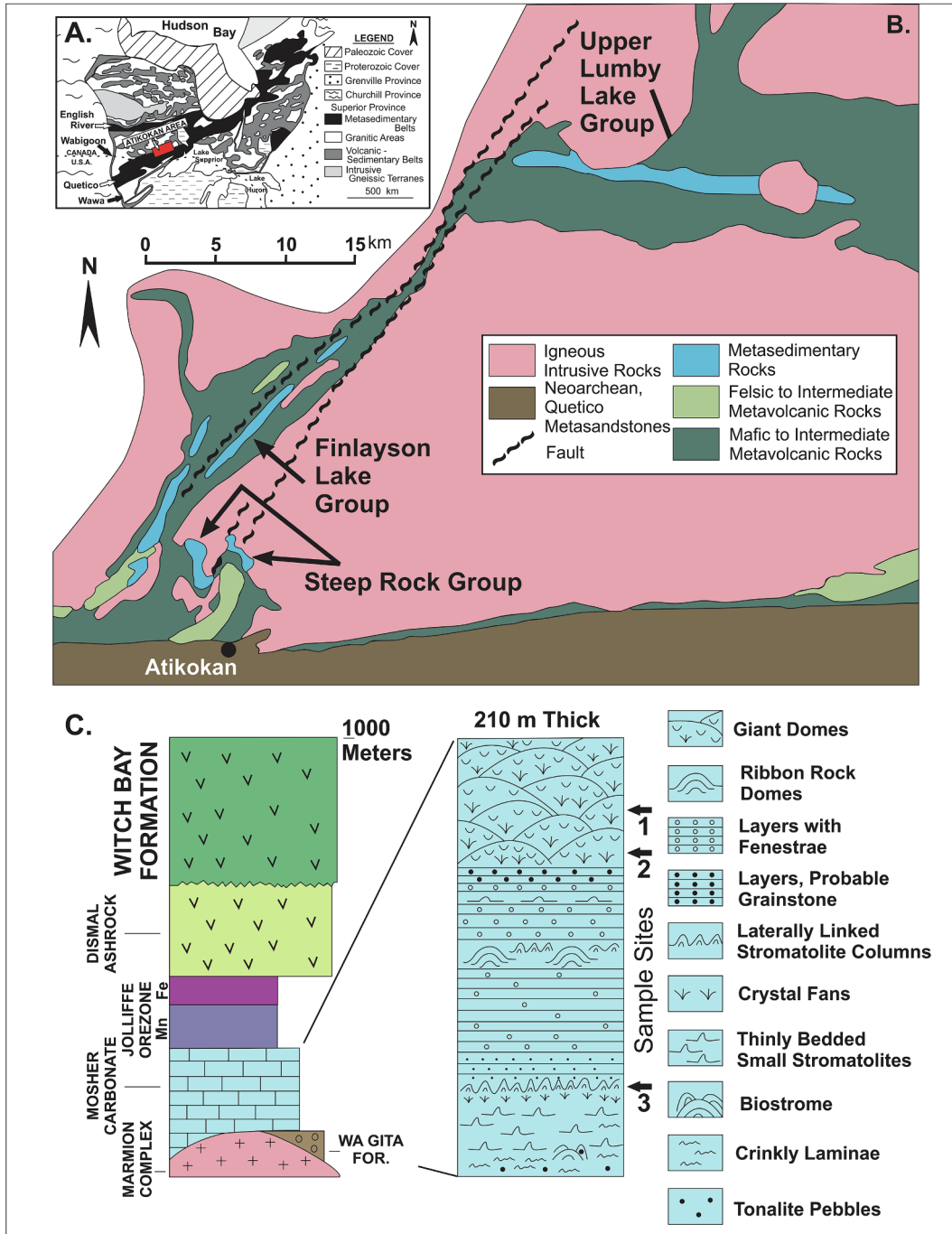


Fig. 1. (A.) Canadian Shield with study area in red. (B.) Location of the Moshier Carbonate, Steep Rock Group on the southern edge of the Wabigoon Subprovince, Superior Province. The Wagita Formation, underlying the Moshier Carbonate (C.), is a sandstone-conglomerate fluvial succession filling paleovalleys in the underlying 3.0 Ga tonalite. It transitions laterally into the Finlayson Lake Group, a nearshore siliciclastic assemblage with small coarsening upward delta lobes. A fault truncates the delta top assemblage, eliminating the Moshier Carbonate. Further to the northeast in the western portion of the Upper Lumby Lake Group, sandstones coarsen upwards into conglomerate, which are overlain by carbonate. Iron formation caps the sedimentary succession. Eastward in this assemblage, first carbonate and then siliciclastics pinch out, leaving only iron formation overlying tonalite. (C.) Stratigraphic succession showing Moshier Carbonate platform lithofacies and the position of the three sites where samples were collected: Site #1 is at 15U 600360 m E and 5405653 m N; Site #2 is at 599763 m E and 5407955 m N; Site #3 is at 599851 m E and 5407948 m N. These correspond to locations 6, 2 and 1, respectively, of Fralick and Riding (Fig. 4, 2015).

lagoons can slow precipitation rates and also alter the minerals that form from solution. More extreme relative sea-level fall can modify platform interior sediments and subaerially expose nearshore and also platform rim deposits. Continued relative sealevel fall can also expose the platform interior sediments. Resultant exposure to meteoric water leading to dissolution, cementation and replacement reactions will further alter carbonate geochemistry and mineralogy. Although numerous detailed studies have documented these effects in Phanerozoic carbonates (James and Choquette, 1983a, 1983b, 1984; Emerson and Hedges, 2004; Morse, 2004; James and Jones, 2016), investigations of diagenesis-induced chemical variability in Precambrian, and especially Archean, carbonates are much less common (e.g. Franchi, 2018, and references therein).

In one of the few studies to examine chemical variability in Archean carbonates, Veizer et al. (1982) assessed relative degrees of alteration in fifteen successions. They concluded that the ~2.8 Ga Mosher Carbonate at Steep Rock Lake (Fig. 1), was the least altered. This is supported by pristine carbon (C) isotope (Fralick and Riding, 2015) and strontium (Sr) isotope values (Satkoski et al., 2017) indicating that these limestones have not experienced alteration capable of causing exchange reactions between the limestone and fluids with differing Sr and C isotopic ratios. Additionally, no evidence of significant Precambrian sub-aerial exposure, with the exception of possible desiccation cracks developed on a giant dome surface (Fig. 20C in Fralick and Riding, 2015; Fig. 7 in Kurucz and Fralick, 2018), suggests that meteoric alteration may not have affected these sediments. These attributes make the Mosher Carbonate a prime candidate for the study of chemical variability caused by changes in water mass geochemistry during carbonate precipitation. Furthermore, differences in $\delta^{13}\text{C}$ and abundances of Ce, Sr, Ba, Mn, and Fe that correlate with lithofacies occur in whole rock samples (Fralick and Riding, 2015), and possibly also in Mosher Carbonate hardgrounds (Kurucz and Fralick, 2018). These studies highlighted a relationship between lithofacies and geochemistry, but lacked the precision to explore this further. Here we employ microanalysis techniques that allow further scrutiny of these relationships, thereby offering the possibility of developing an understanding of the evolutionary history of the water-masses that these carbonate and siliceous minerals precipitated from.

2. Methodology

2.1. Analytical

Samples were obtained from three different areas in the disused workings of the Steep Rock iron mine where the Mosher Carbonate forms the footwall. Sample Site #1 is on the north side of Errington Pit (Locality 8 in Wilks and Nisbet, 1985, 1988; Locality 6 in Fralick and Riding, 2015). This is the most pristine of the three sites, with mm-scale sedimentary structures clearly discernible and no visible evidence of alteration in the carbonates. Site #2 is on the shore of the lake occupying Hogarth Pit (Locality 4 in Wilks and Nisbet, 1985, 1988; Locality 2 in Fralick and Riding, 2015). The samples were collected 15 m from a 40 m wide hematized zone that is stratiform with the vertical bedding and probably formed during Cretaceous sub-aerial weathering (Kimberley and Sorbara, 1976; Machado, 1987). Site #3, inland from the hematized zone (Locality 3 of Wilks and Nisbet, 1985, 1988; Locality 1 of Fralick and Riding, 2015), consists of a bed of dolostone surrounded by limestone. The rocks sampled in these three areas lack visual signs of alteration, aside from recrystallization of the carbonate into a mosaic of blocky crystals, probably during the 2.7 Ga Kenoran Orogeny.

The terrain sampled was repeatedly glaciated during the Pleistocene and most samples came from previous working faces of the open pit iron mines in the area. Thus, the sampled outcrops were relatively fresh, with weathering rinds only extending a maximum of millimeters into the rock. Two of the seven samples used were dolomite with diagenetically reset Sr isotopes. The other five samples are limestone with Sr isotopes

that reflect Mesoarchean seawater values (Satkoski et al., 2017). Large samples were slabbed and polished for scanning that was performed on a high resolution XRF scanner at the European Institute for Marine Studies, Plouzané, France. Areas in the samples with small-scale lithofacies transitions were identified, extracted with a trim saw, and processed to produce standard size polished thin sections 100 to ~120- μm thick. These were used to analyze major and trace element contents of laminae composed of different carbonate lithofacies. Rare earth elements (REEs) together with yttrium (Y), silicon (Si), manganese (Mn), iron (Fe), strontium (Sr), and barium (Ba), were analyzed by laser ablation – inductively coupled plasma – mass spectrometry (LA-ICP-MS) at the Department of Geosciences, University of Bremen, Germany, using a New Wave UP193 laser coupled in-line to a Finnigan ELEMENT 2 mass spectrometer. The laser was operated with a pulse rate of 5–10 Hz at ca. 1.3 GW/cm² irradiance to sample 100 μm points along lines across lithofacies, using helium as carrier gas and argon as added make-up gas (both at ca. 0.8 l/min.). The analyzed areas were pre-ablated with a 120 μm beam diameter at approximately 0.3 GW/cm² irradiance to avoid surface contamination. For data reduction, Cetac Geopro™ software was applied using NIST612 (REE + Y) and NIST610 (Si, Mn, Fe, Sr, Ba) as external calibration standards (Pearce et al., 1997; Jochum et al., 2005) and ⁴³Ca as an internal standard element (assuming a sample calcium content of 40.00 wt%). A detection limit of 0.001 μg was tentatively assigned given the low blank signals. Analytical precision and accuracy were monitored by repeated standard analyses (USGS BCR-2-G). For REE + Y, precision and accuracy is better than 8 % (and better than 5 % for most REEs). While Mn, Sr, and Ba yielded 2–11 %, Mg and Fe yielded significantly lower values between 14 and 40 %. Ba/Eu ratios were almost all under 500 with few reaching as high as 4700, negating problems with BaO interference (Zepeda et al., 2024). REE anomalies were calculated using the equations of Bau and Dulski (1996), specifically designed for Archean carbonates and iron formations: for the Ce anomaly $\text{Ce}^* = \text{Pr}/(0.5\text{Ce} + 0.5\text{Nd})$, which eliminates the problem of using La in the equation, with its positive anomalies, and for the La anomaly $\text{La}^* = \text{Ce}/(0.5\text{La} + 0.5\text{Pr})$. The equation put forward for Ce* by Lawrence et al. (2006) produces similar results (see data repository). (Note: Using Bau and Dulski's (1996) equation a negative Ce anomaly will be less than 0.95. Whereas, using Lawrence et al. (2006) a negative anomaly will be above 1.05). Error limits of these equations are those of Planavsky et al. (2010). Normalization of these values utilized division by Post Archean Australian Shale (PAAS) (Taylor and McLennan, 1985).

2.2. Sampling strategy

Knowledge of original carbonate mineralogy is critical to understanding diagenetic evolution. Aragonite is metastable and will transform to calcite over time. However, due to the high partition coefficient of Sr favouring aragonite over calcite during both abiotic (Kinsman, 1969; Kinsman and Holland, 1969) and biotic (Dietzel et al., 2004) precipitation, modern aragonite typically contains thousands of ppm Sr. During recrystallization into calcite some Sr is lost, but enough commonly remains to allow identification of those calcites as originally aragonite (Katz et al., 1972). Barium behaves in a similar manner, but to a lesser extent (Rimstidt et al., 1998; Mavromatis et al., 2018). Thus, Sr and Ba concentrations were analyzed using LA-ICP-MS, and, in addition, Sr was mapped by XRF. High concentrations of Sr indicate that the carbonate was probably originally aragonite as Sr fits into the aragonite lattice better than the calcite lattice (Bathurst, 1975). Iron, magnesium and manganese behave in the opposite manner, preferentially fitting into the calcite lattice. So these were also analyzed using LA-ICP-MS, and XRF mapped.

Previous investigation of REE concentrations indicated that free oxygen was present on the Steep Rock carbonate platform, as revealed by pronounced negative Ce anomalies (Riding et al., 2014; Fralick and Riding, 2015). This has been considered by some the most compelling Ce anomaly evidence for free oxygen in the older Precambrian (Zhang and

Shields, 2022; also see this reference for in depth discussion of the use of Ce anomalies as proxies for oxygenation). The diagenetic processes these rocks have been through have far-reaching importance for understanding ocean–atmosphere geochemistry during this time interval. Whether the negative Ce anomalies some of these rocks exhibit (Riding et al., 2014; Fralick and Riding, 2015) are primary, or are artefacts of post-depositional processes, was explored using LA-ICP-MS to evaluate the exact location of the anomalous Ce concentrations. The REE europium (Eu) is also useful in deciphering ancient water body migration (Bau and Dulski, 1996; Kamber and Webb, 2001). As hydrothermal fluids travel through the mafic seafloor, Eu^{2+} in the rocks can undergo replacement reactions with cations in solution (Derry and Jacobsen, 1990; Danielson et al., 1992). This has caused Archean open ocean water, and deep water in particular, to have positive Eu anomalies when normalized with PAAS, as noted by many authors working on Archean chemical and biochemical sediments (Barrett et al., 1988; Bau and Moller, 1993; Alibert and McCulloch, 1993; Bau and Dulski, 1996; Kamber et al., 2004; Bolhar et al., 2004; Bolhar et al., 2005; Bolhar and Van Kranendonk, 2007; McIntyre and Fralick, 2017; Afroz et al., 2023).

3. Regional setting

The Steep Rock Group occurs near the southern border of the Wabigoon Subprovince in western Superior Province, Ontario, Canada. It was formally defined by Wilks and Nisbet (1988) as containing five formations (Fig. 1). The lowest of these is the Wagita, which sporadically

fills depressions in the 3003 ± 5 Ma (Davis and Jackson, 1988; see also, 3003 ± 3 Ma Tomlinson et al., 1999 and 3001.6 ± 1.7 Ma Tomlinson et al., 2003) tonalite basement. Its conglomerates and sandstones represent river deposits that formed small prograding delta lobes in the Finlayson Lake Group (Fig. 1) (Fralick et al., 2008).

A flooding surface brought this depositional style to an end as the Mosher Carbonate (Fig. 2) transgressed from offshore waters of the Upper Lumby Lake Group (Fig. 1). There is disagreement about the thickness of the Mosher Carbonate in the Steep Rock area. Early work (Smyth, 1891) placed the thickness at 150–200 m, whereas later estimates range from 300 m (Jolliffe, 1955) to 500 m (Wilks and Nisbet, 1985). It has been divided into two members (Fralick and Riding, 2015). The lower Hogarth Member consists of pseudocolumnar (Fig. 3A,B), coniform, domal-stratiform (Fig. 2D) and stratiform stromatolites; together with fenestral fabric; thrombolite-like fabric; banded limestone, sheet cracked limestone; crystal fan fabric; and grainstones. These have been interpreted as having been deposited in the interior (Riding et al., 2014; Fralick and Riding, 2015) of an isolated, rimmed carbonate platform (Fralick et al., 2008) formed on an oceanic volcanic plateau (Wyman and Hollings, 1998; Hollings and Wyman, 1999; Hollings et al., 1999). The overlying Elbow Point Member consists of giant hybrid carbonate domes (Fig. 2A,B) made of alternating crystal fan fabric (Fig. 3D,E), cusped (Figs. 2C and 3C) and net-like fenestral fabric (Fig. 2C, 3C,D,E), and thin iron-rich layers, and are interpreted to have formed the outer rim of the carbonate platform (Fralick and Riding, 2015; Riding et al., 2022).

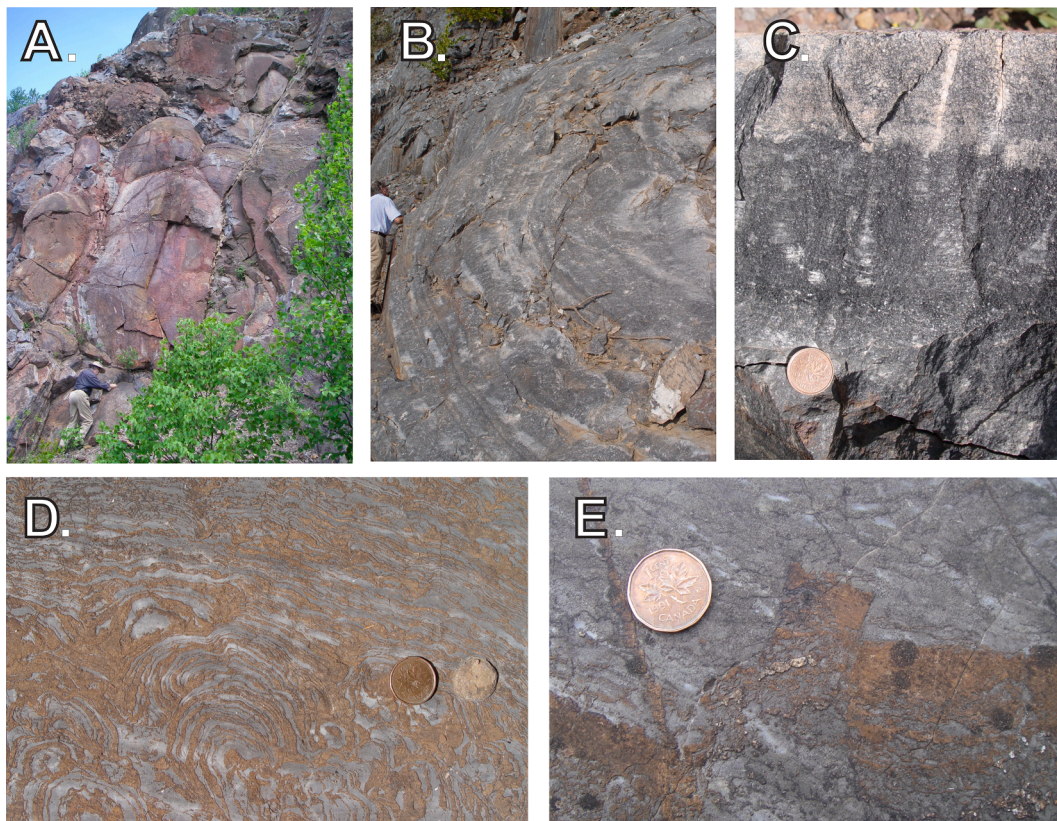


Fig. 2. Mosher Carbonate lithofacies. Way-up is to the top except in A and B. (A.) Giant hybrid carbonate domes at sample Site #2 (site locations on Fig. 1C). Strata are near vertical. This view shows the top surface of the domes. (B.) Cross-section through giant hybrid carbonate domes at sample Site #1. Way-up is to the left. Carbon in crystal fan fabric and cusped fenestral microbialite layers imparts the dark tint, whereas net-like fenestral carbonate layers with larger amounts of void filling cement form the grey layers. (C.) Close-up view of dark cusped fenestral fabric and grey net-like fenestral microbialite layers with abundant blocky cement. Site #1. Coin is 1.9 cm. across. (D.) Domal-stratiform biostrome with laterally linked concentric domes, Site #3. Laminae alternate between grey calcite and orange ferroan dolomite that probably formed by replacement of calcite (Fralick and Riding, 2015). (E.) Top-down ferroan dolomite replacement of a calcite bed, Site #3. The flat upper surface and irregular lower surface of the layer is consistent with alteration caused by overlying seawater. A multitude of ferroan dolomite replacement zones exhibit these characteristics. Dewatering structure displacing ferroan dolomite into the overlying limestone layer attests to the early nature of the replacement, which likely occurred at the seafloor (Fralick and Riding, 2015).

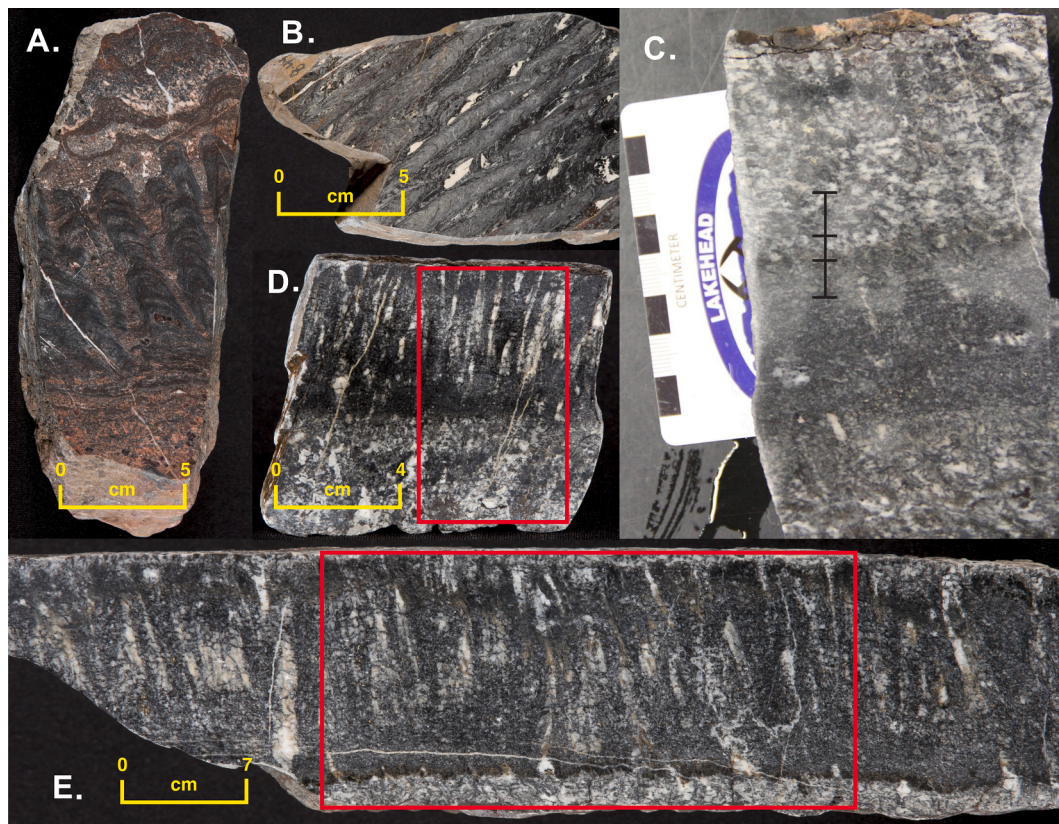


Fig. 3. Examples of samples used in this study (up is to top of photos except B where it is to top right): (A., B.) Samples 8–43 and 8–44, respectively, showing narrow columnar stromatolites with bridging laminae, subparallel branching and walled structure, from a ferroan dolomite horizon, Site #3. (C.) Sample SR-20, from Site #1. The lower half shows net-like fenestral microbialite overlain by dark cusped fenestral microbialite. A very dark, 0.5 cm wide contact area separates the cusped fenestral microbialite from another net-like microbialite that overlies it. The black line marks the LA-ICP-MS track (Figs. 10 and 11) with the lower, middle and upper portions differentiated. The scale on the left is in cm. (D.) Sample Sr-16, Site #1. The base is composed of net-like fenestral microbialite, and the top half is composed of a single layer of crystal fans. They are the sub-vertical black areas with white cement between them. The red square marks the area of the XRF scan (Fig. 5). The LA-ICP-MS line of analytical spots was run horizontally across the dark fans and white void filling cements (Fig. 6). (E.) Sample SR-18, Site #1. Net-like fenestral microbialite at the base is separated from crystal fans by a thin dark layer. Red rectangle is the area scanned for XRF analyses (Fig. 4). Carbon in crystal fan layers and cusped fenestral microbialite layers imparts the dark tint, whereas net-like fenestral microbialite layers with larger amounts of void filling cement form the grey layers.

The Steep Rock carbonate thins to the northeast until it disappears and the iron formation that overlies it rests directly on underlying basalts and komatiites of the ocean plateau (Fralick et al., 2008), whose upper level has a U-Pb age of 2831 ± 2 Ma (Tomlinson, et al., 2003). As rate of subsidence and/or absolute sealevel rise outpaced rate of deposition, a transgressive systems tract developed and the area was progressively flooded from the northeast to the Steep Rock area in the southwest. The deeper water sediments that encroached from further offshore consist of 100 to 300 m of manganiferous iron formation (Wilks and Nisbet, 1988), with MnO contents averaging 3.78 wt% and up to 19 wt% (Huston, 1956). These were deposited directly on the limestones and grade upward into 50 to 100 m of iron formation (Wilks and Nisbet, 1988) with less than 0.5 wt% MnO (Huston, 1956). Sediment deposition terminated prior to 2780.2 ± 1.4 Ma (Tomlinson et al., 2003) when pyroclastic komatiite eruptions deposited 100 to 400 m of ash and blocks in the Steep Rock area (Wilks and Nisbet, 1988).

4. Results

4.1. Site #1

At this site (Fig. 1C) the upper Elbow Point Member limestones consist of giant hybrid domes (Fig. 2B) with layers of net-like fenestral microbialite, cusped fenestral microbialite (Fig. 2C, 3C) and crystal fan fabric (Fig. 3D). They are located, at a minimum, hundreds of meters

from carbonates showing visible evidence of alteration in the form of being cut by large oxidation pipes. These pipes consist of hematite, goethite, pyrolusite and angular blocks of dolomite with dolomite cements. The assemblage has not been metamorphosed and the oxides are unconsolidated in places. Though the carbonates distal from any pipes are quite coarse grained, probably due to lower greenschist metamorphism (Nisbet and Wilks, 1989), the sedimentary structures are readily visible, highlighted by the carbon in the rocks. Carbonate $\delta^{13}\text{C}$ values range from 1 to 2.5 (Fralick and Riding, 2015) and Sr isotopic ratios of 0.7018 reflect late Mesoarchean seawater (Satkoski et al., 2017). The following describes the geochemistry of the sedimentary structures present at this site.

4.1.1. Crystal fan fabric (Fig. 3D, E)

The crystal fan fabric consists of 5 to 20 cm tall, commonly upward radial clusters of millimetric to centimetric carbonate crystals up to one or two cm thick (Fralick and Riding, 2015, p. 152). They have elevated amounts of Sr and Ba (Figs. 4, 5, 6, 7), though the inter-crystal cements have less, on average, than the fans (Figs. 6 and 7). They also have lower amounts of iron and manganese (Figs. 4 and 8) compared to other lithofacies at this site, and all obtained REE patterns of the 44 LA sampling spots of this fabric, except one, have negative Ce anomalies (Figs. 5 and 9). The fans commonly grow upwards from thin silica-rich layers (Fig. 4), which have higher concentrations of Mn in the carbonate phase and Fe, Al and K present in sericite and subordinate iron oxides. The

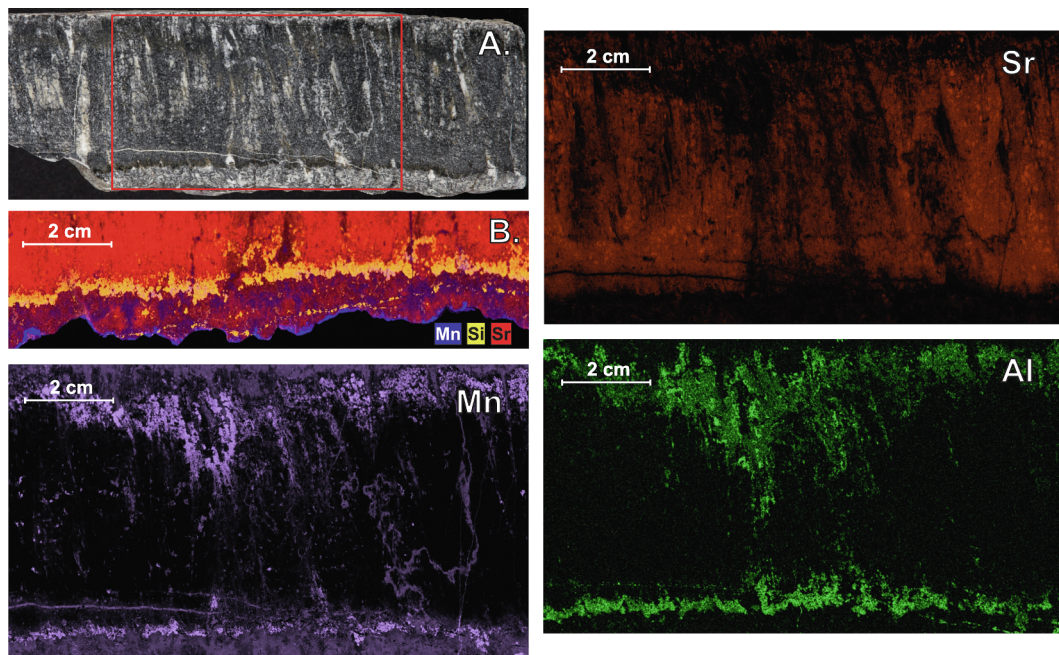


Fig. 4. (A.) Net-like fenestral microbialite overlain by thin, dark laminae from which crystal fans grew (limestone sample SR-18 from Site #1, Fig. 3E). The crystal fan fabric is overlain by net-like fenestral microbialite. The red rectangle is the area of the XRF false colour elemental scans, and is ~ 10 cm wide. (B.) XRF false colour imagery shows that the net-like fenestral microbialite in the basal portion of A is Mn-enriched calcite with insignificant ferroan dolomite (with Mg, Fe, Mn), siliciclastics (Al, K, Ti), and chert (Si). This is sharply overlain by a thin layer mostly containing Si. Aluminum and K are also present in sericite in addition to iron oxides (Fe and Mn). Crystal fans grew up from this layer. Sr is concentrated in the crystal fans with lower, to much lower, amounts in the cement filled voids separating them. Mn and Al (also Fe, Mg, K and Ti, not shown) are associated with the upper surface of the crystal fans. Note that the upper net-like fenestral microbialite horizon is compositionally similar to the lower one.

upper surface of the fans is irregular, with increasing amounts of Mn, Fe, Si, Al, K and Ti (Figs. 4 and 5) present in ferroan dolomite and aluminosilicates. In sample SR-16 thin Mn, Fe dolomite veins cut these lithofacies without the presence of elemental haloes in the adjacent rock (Fig. 5)

4.1.2. Cuspate fenestral microbialite fabric (Fig. 2C, 3C)

This fabric consists of nested, flattened, lensoid, concave-up fenestrae, a few mm to 2 cm wide and up to 2 mm in height, delineated by thin, fine-grained draping laminae, commonly between well-defined vertical supports (Fralick and Riding, 2015, p. 153; also see Sumner, 1997a). The calcite in this fabric has an elevated concentration of Sr and Ba, with a low amount of Fe and Mn compared to the net-like fabric and the stromatolites (Figs. 7, 8, 10, 11). The majority of sampled areas also have significant negative Ce anomalies with values similar to those of the crystal fan fabric (Fig. 9). Laminae with large amounts of Fe, Mg, Mn forming ferroan dolomite crystals, Si in quartz and Al, Ti and Si in siliciclastics separate some layers of cuspate fenestral microbialite from net-like fenestral microbialite. In other areas the laminae separating these are simply enriched in Si, Al and Ti, or the net-like fabric may grade into the cuspate fabric without any intervening Si, Al enriched laminae

4.1.3. Net-like fenestral microbialite fabric (Fig. 2C, 3C, D, E)

This fabric is dominated by millimetric, irregularly shaped fenestrae with thinner dark contorted laminae separating them. The chemistry is dominated by the cement in the fenestrae which make up the majority of the fabric. It is composed of calcite with relatively low amounts of Sr, Ba, Mg, Si, Al, K and Ti and intermediate to low amounts of Fe, Mn and Mg (Figs. 4, 5, 7, 8), though it can contain Si-rich laminae (Fig. 10B). It is the only lithofacies where the vast majority of samples had more Mn than Fe (Fig. 8). The LA-ICP-MS analyzed points in the net-like fabric in sample SR-20 show positive to negative Ce anomalies, whereas those in the net-like fabric of sample 16 mostly have positive Ce anomalies (Fig. 9). This layer also has veins and extensive irregular areas rich in Mn. The

contacts of the layers of net-like fabric with other layers are described above

4.2. Site#2

This site consists of limestone in the Elbow Point Member's basal strata (Fig. 1C). These are located 15 m from a vertical, stratiform oxidized alteration zone, probably formed during Cretaceous exposure (Kimberley and Sorbara, 1976; Machado, 1987). The giant hybrid domes located here (Fig. 2A) are easily accessible and often occur in textbook photographs of Steep Rock "stromatolites". Similar to Site #1 they have hybrid fabrics composed of interlayered net-like fenestral microbialite, cuspate fenestral microbialite and crystal fan fabric.

4.2.1. Crystal fan fabric (Fig. 12)

Groups of crystals in the crystal fan fabric are Sr-rich. Mn-bearing veins cut through them and are associated with a speckling of Mn-rich calcite crystals replacing the Sr-rich calcite

4.2.2. Cuspate fenestral fabric (Figs. 12, 13)

At this location some layers of cuspate fenestral fabric are Sr-rich, but they commonly laterally and vertically grade into areas with extensive Mn-rich veins and adjacent Mn-flooding (Figs. 12B, 13B). These layers are separated from net-like fenestrae and crystal fan fabric by silica-rich horizons

4.2.3. Net-like fenestral fabric (Figs. 12, 13)

The net-like fabric exhibits various degrees of replacement by Mn-rich calcite. Some layers have irregular blotches of this alteration superimposed on the layers of calcite (Fig. 12), whereas others have a similar blotchy Mn-rich calcite pattern with the entire layer flooded by lesser amounts of Mn (Fig. 13). Remnant crystal fan fabric can be seen in some of the net-like fenestral fabric

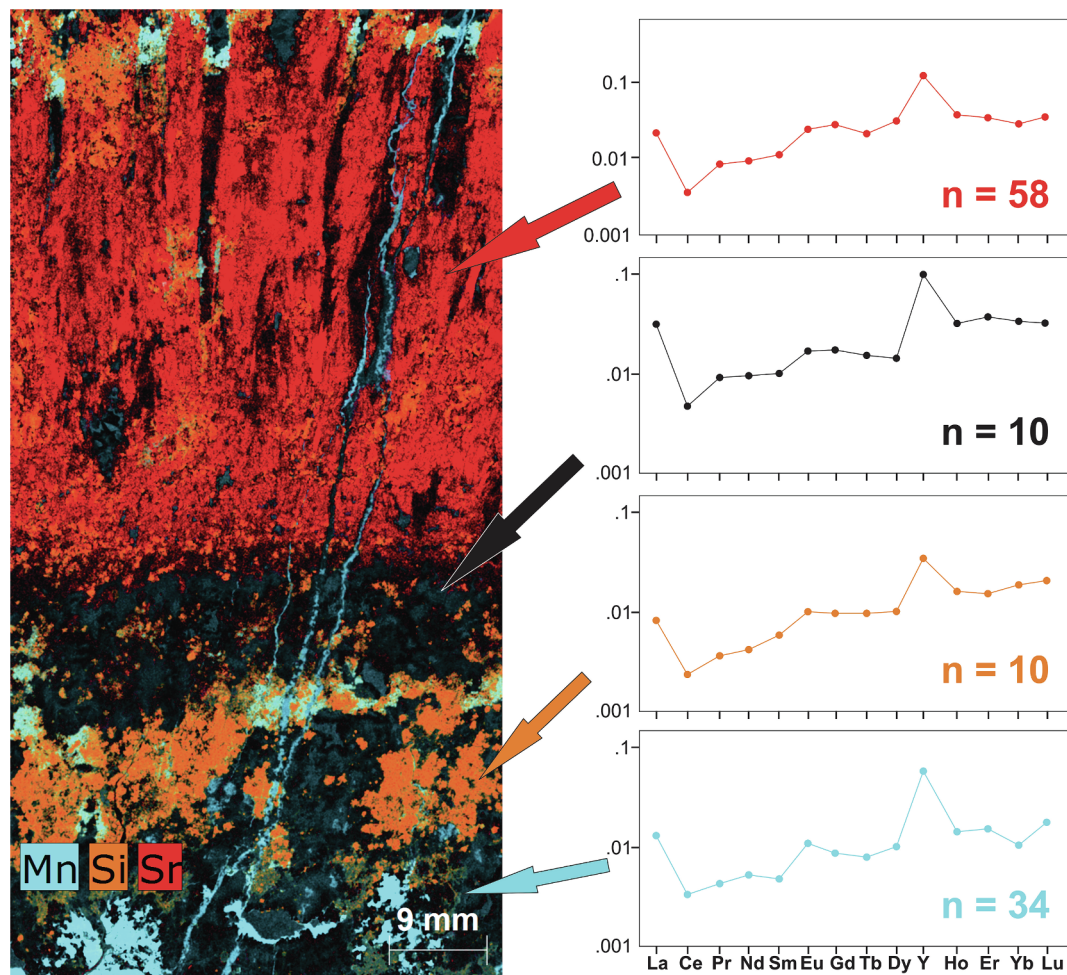


Fig. 5. XRF false colour image of limestone sample SR-16 (Fig. 3D) from Site #1. The lowest laminae (blue arrow) of net-like fenestral fabric has low amounts of Sr and Si with veins and large secondary vugs filled with significant amounts of Mn (Blue), Fe and Mg, with some Ca and S. These are overlain (orange arrow) by a 1 cm wide Si-rich laminae (Pink) incorporating even larger amounts of Al, Fe, Mn and Mg that increase in concentration upward through the layer (Light Blue areas). The third layer (black arrow) has much less Si, Fe, Mg and Mn making it black, although Sr, Si, Mn and Al concentrations increase at the top of this layer (Light Scarlet to Red). It is overlain by the Sr-rich crystal fans (red arrow) with areas replaced by quartz (orange), particularly near their apices. Mn contents are higher in the inter-fan areas, and near the tops of the fans plugs composed of Fe, Mn, Mg and Si fill the inter-fan areas (Light Blue). All layers have positive Y and La anomalies. The two lowest layers lack a Ce anomaly, but have a Eu anomaly, although it is very minor for this Si-rich layer. The two upper layers have negative Ce anomalies but no Eu anomaly.

4.3. Site #3

Site #3 is in the Hogarth Member which represents the interior (Fralick and Riding, 2015) of this isolated carbonate platform (Fralick et al., 2008) and consists of various types of stromatolites, fenestral fabric, banded limestone, grainstone and atikokania crystal fans. The two samples studied here are from a 25 cm thick, ferroan dolomite bed of narrow stromatolite columns (Fig. 3A, B). This bed has sharp contacts with limestones on either side and was the only ferroan dolomite bed encountered, though ferroan dolomite laminae are common. The laminae probably formed as a replacement of calcite by incursions of off-platform seawater, and it was assumed that this thicker unit similarly was formed from a larger flooding event (Fralick and Riding, 2015; Riding et al., 2022).

4.3.1. Stromatolites (Fig. 3A, B)

The columnar stromatolites have been extensively replaced by quartz (Fig. 14C). Some portions of the stromatolites and bridging laminae are ferroan dolomite (shown by concentrations of Ca, Mg, Fe and Mn), but most ferroan dolomite is in interdigitate cements (Fig. 14B). Although this general trend exists, the overall LA-ICP-MS

elemental distributions are somewhat chaotic (Fig. 15). Sr values comparable to those in nearby calcite beds are present in some dolomite layers (Fig. 16B), accompanied by positive Ce anomalies (Fig. 16E). Calcite laminae (low Mg concentrations, Fig. 15 C and 16C) have the lowest Sr values, substantially lower than adjacent dolomite and surrounding limestone beds. The Ce anomaly (Fig. 15E, 16E) is dominantly between 0.95 and 1.05, which is within error limits of 1.0 and cannot be used to infer anomalies (Planavsky et al., 2010). Regardless, two of the 69 LA sampling sites had a statistically significant negative Ce anomaly and 15 had positive ones

4.4. LA-ICP-MS data overview

Considered as a whole, the LA-ICP-MS data reveal several trends. The crystal fans contain the greatest amount of Sr and Ba, while the blocky cement between them on average has less (Fig. 7). The dark layer forming the base of the fans, and the majority of the cusped fenestral microbialite in SR-20 have Sr concentrations similar to the cements between the crystal fans. The remaining samples from the cusped fenestral microbialite in SR-20, those from the dark Fe- and Si-rich middle layer in SR-20, and from the net-like fenestral microbialite

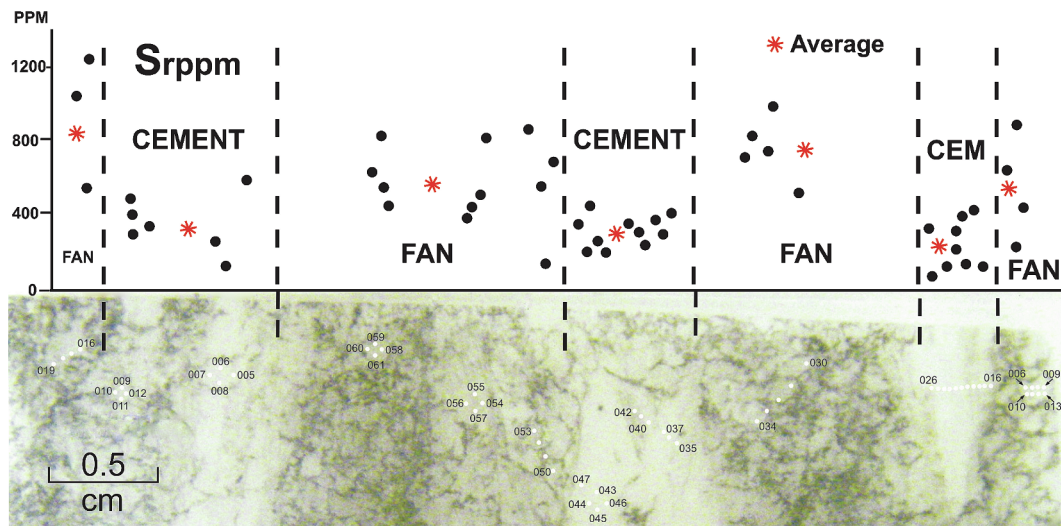


Fig. 6. Limestone sample SR-16, upper portion of Fig. 3D and 5. A series of 58 LA-ICP-MS point analyses were acquired horizontally across the upper crystal fan fabric to compare the geochemistry of the crystal fans with the inter-fan cements. Visually, the fans are enriched in carbon that is concentrated between the constituent calcite crystals, whereas the calcite in inter-fan areas appears white with lower amounts of carbon. Average Sr and Ba contents are higher in the fans (see also Fig. 7) than in the cement, which on average, is higher in Fe, Mn, Mg, and Si (Fig. 8). Data from individual crystals, e.g. the analyses of the crystal in the fan on the far right, can show a great deal of heterogeneity.

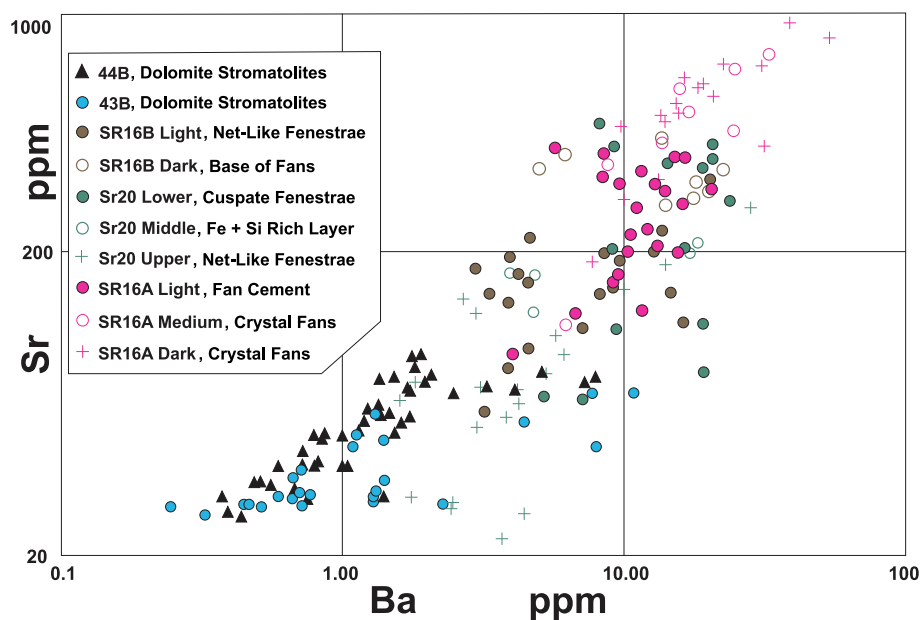


Fig. 7. Sr vs Ba cross-plot of all the LA-ICP-MS data. The crystal fan fabrics have the greatest amount of Sr, and are also enriched in Ba compared to other samples. The analyses of crystal fan cements plot at lower Sr levels but generally have comparable amounts of Ba. The area where the crystal fan cements plot also contains points derived from the layer at the base of the crystal fans in sample SR-16 and from the dark cusped fenestral microbialite in sample SR-20. The middle area of the plot is mostly occupied by analyses of the net-like fenestral microbialite shown in the lower half of sample SR-16 and, slightly below this, the net-like fenestral microbialite in the upper portion of SR-20. Data from the Fe- and Si-rich thin dark laminae in Sample SR-20 also mostly plots in this area. The samples with the lowest Sr and Ba contents are from the ferroan dolomite columnar stromatolites.

layer in SR-16B, plot in an intermediate range of Sr and Ba. The net-like fenestral microbialite layer in SR-20 plots from this area towards the low end of the graph, and the lowest values were from the ferroan dolomite stromatolite samples 8–43 and 8–44.

A scatterplot of Fe vs Mn (Fig. 8) shows an opposite trend to Fig. 7, with the dolomite samples having the largest values and the crystal fans the lowest. The other samples congregate in the middle of the diagram. A line through Fe/Mn = 1 separates the limestone data into two groups: the crystal fans and their associated cement have most of their samples above the line, and samples of the dark layer forming the base of the fans

also occupy the Fe greater than Mn field. Both groups have negative Ce anomalies (Fig. 17). The majority of the samples from the net-like fenestral microbialite in SR-16B and all the samples in the net-like fenestral microbialite layer in SR-20 are enriched in Mn compared to Fe (Fig. 8), and these samples mostly have positive to no Ce anomalies (Fig. 9). The majority of the stromatolitic ferroan dolomite samples also lack Ce anomalies. In summary, therefore, there are three groups: (1) Layers with negative Ce anomalies and Mn/Fe less than 1; these include (a) crystal fan fabric, (b) the layer forming the base of the crystal fans, and (c) the cusped fenestral fabric. (2) Layers with no to positive Ce

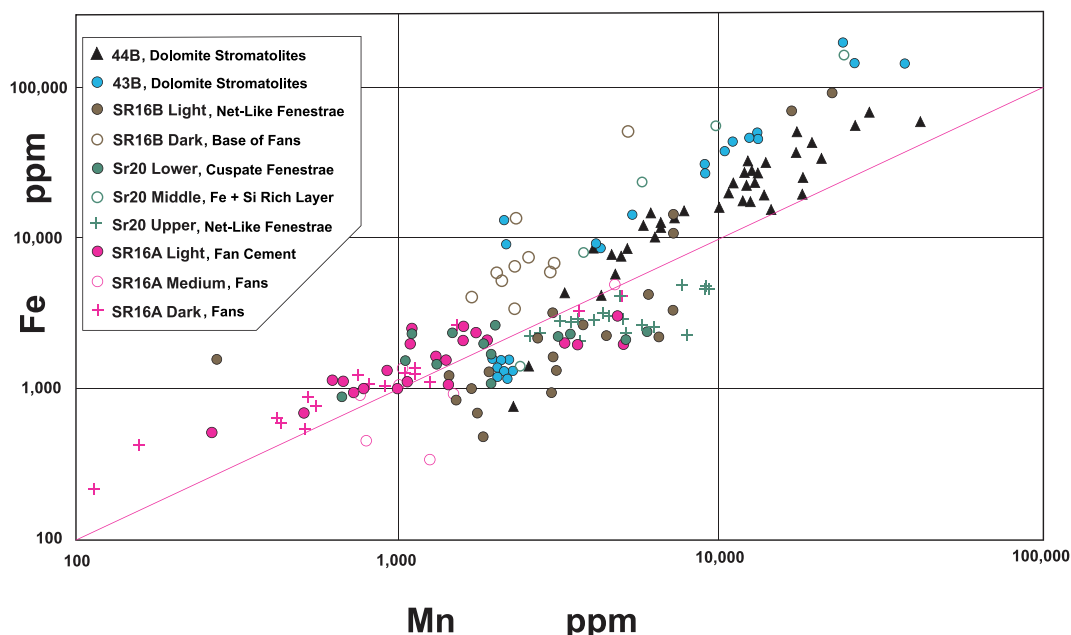


Fig. 8. Fe vs Mn cross-plot of all the LA-ICP-MS data. From upper right to lower left the data array extends from ferroan dolomite columnar stromatolites (44B and 43B) with high values, to crystal fans and their cements, with low values. The other samples cluster between these two end members. The line denotes the same amount of Fe and Mn in the sample (Fe = Mn). Samples from the net-like fenestral microbialite of SR-16B, the net-like fenestral microbialite of SR-20 and a cluster of ferroan dolomite analyses from sample 43B, plot below this line indicating that their carbonate is enriched in Mn compared to Fe. The net-like fenestral samples have abundant cement compared to samples plotting above the line with Mn/Fe ratios above one. These are also the samples that have positive to no Ce anomalies. In contrast, most of the calcite samples that plot above the line, and therefore have more Fe than Mn in their crystal lattice, have negative Ce anomalies.

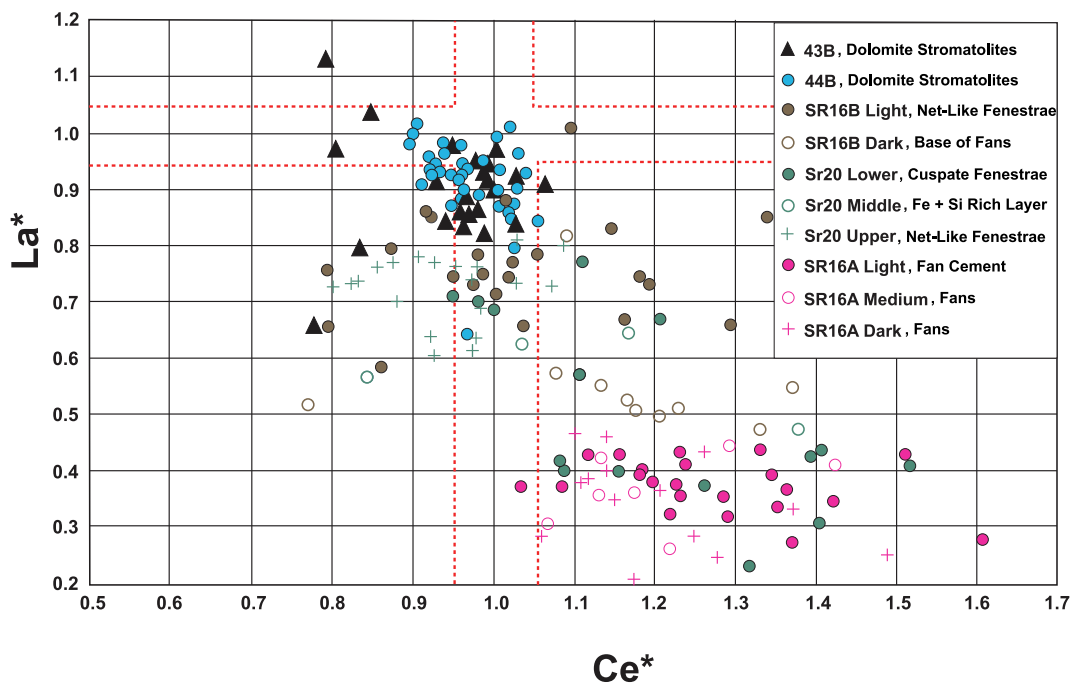


Fig. 9. Plot of Ce anomaly ($Ce^* = Pr / (0.5Ce + 0.5Nd)$) vs La anomaly ($La^* = Ce / (0.5La + 0.5Pr)$) (Bau and Dulski, 1996). All values have been normalized to PAAS (Taylor and McLennan, 1985). Within the red lines there are no significant Ce or La anomalies (Planavsky et al., 2010). Only 4 of the 43 analyses of crystal fans and their cement lack negative Ce anomalies. A considerable majority of the samples from the base of the crystal fan layer in SR-16B and the cusped fenestral microbialite layer in SR-20 also have negative Ce anomalies. This contrasts with the net-like fenestral microbialites of samples SR-16B, SR-20 and the columnar stromatolite ferroan dolomite samples (43B, 44B), which seldom have negative Ce anomalies. Highlighting this difference, half of the analyses of the net-like fenestral microbialite of SR-20 have positive Ce anomalies.

anomalies and Mn/Fe ratios greater than 1; these are the net-like fenestral microbialite layers with large blocky cement crystals. (3) The ferroan dolomite stromatolites whose majority of samples are enriched

in Fe more than Mn and have no Ce anomalies, similar to Fe-rich precipitates formed offshore from the carbonate platform.

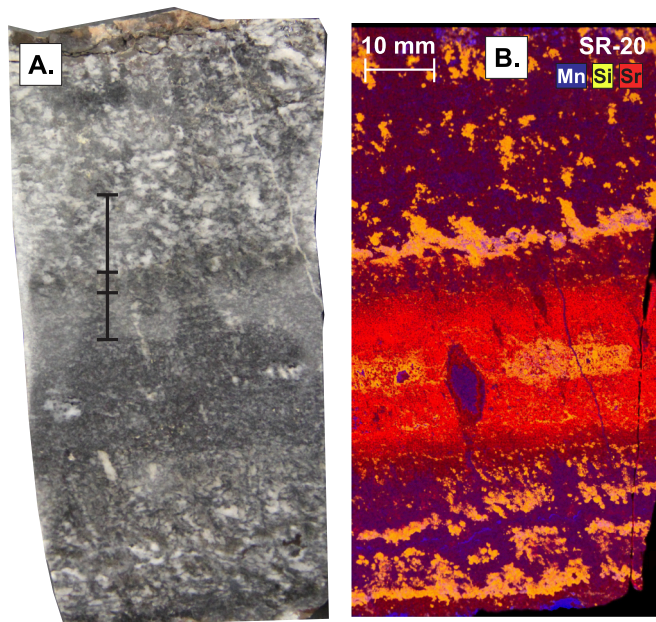


Fig. 10. (A.) Sample SR-20 (Fig. 3C) from Site #1. The black line indicates the track of the laser spots analyzed in Fig. 11. (B.) XRF false colour image of limestone sample SR-20. The lower portion of this limestone sample consists of net-like fenestral microbialite with layers of Mn- and Sr-bearing calcite alternating with Si-rich layers. These Si-rich laminae, including one directly below the Sr-rich area, are also enriched in Al and Ti, but not in Fe, Mg and Mn. Si-rich layers immediately above the Sr-rich area and near the top of the slab are enriched in Fe, Mn, Mg, Al and Ti. The Mn is also concentrated immediately below and above the Fe-rich laminae overlying the Sr-rich area. The net-like fenestral microbialite in the upper third of the slab contains slightly more Fe and Mg than the lower portion.

5. Discussion

Samples used in this study were selected to represent the diversity of both depositional environments and possible alteration histories present in the outcrop area. Samples 8-43 (Fig. 3A, 16, 17) and 8-44 (Fig. 3B, 14, 15, 17) are columnar stromatolites of the central lagoon collected from the only known thick ferroan dolomite layer in the limestone succession (site #3). Samples SR-0 (Fig. 12) and SR-8 (Fig. 13) are calcite crystal fan fabric, cusped fenestral microbialite and net-like microbialite collected from giant hybrid domes on the platform margin (site #2), approximately 15 m from an oxidized area of the limestone. The samples furthest from any areas of extensive oxidation in the limestone (site #1) are SR-16 (Fig. 3D, 5, 6), SR-18 (Fig. 3E, 4) and SR-20 (Figs. 10 and 11). In hand sample this material appears to be similar to site #2 lithologically, texturally, and with comparable sedimentary structures.

5.1. Site #1

This site, apart from very minor amounts of interstitial sediment, is dominated by juxtaposed giant hybrid carbonate domes which are hybrid carbonates largely composed of alternating layers of cusped fenestral microbialite, net-like fenestral microbialite fabric and crystal fan fabric. These layers are commonly separated by thin layers of quartz, aluminosilicates \pm ferroan dolomite and iron oxides. Kurucz and Fralick (2018) interpreted these as alteration/bounding surfaces that possibly formed as sub-aqueous hardgrounds, and separated them into two types. Type 1 occurs at the contacts between net-like microbialite layers and crystal fan fabric. They are dark grey, 0.3–2 cm thick, and consist of microcrystalline quartz intergrown with zoned ferroan dolomite containing iron-rich cores and Mg-rich edges. Iron oxides and

aluminosilicates are also present. Type 2 bounding surfaces are silica-rich thin areas that separate cusped fenestral microbialite from overlying crystal fan fabric. These mainly occur at the base of the fans and grow on the upturned edges of the cusped laminae and their support structures (Kurucz and Fralick, 2018). Silicified areas separate laminae of net-like fenestrae (Fig. 10). These altered zones were probably associated with changing water chemistry that led to replacement of the calcite by ferroan dolomite and silica, and in some layers to precipitation of iron hydroxides (Fralick and Riding, 2015; Kurucz and Fralick, 2018).

The giant hybrid carbonate domes are broadly interpreted as chemocline proximal (Riding et al., 2022). Offshore from them open seawater was precipitating Mn-rich iron formation, whereas in the central lagoon Fe^{2+} contents were low and unable to block calcite precipitation (Riding et al., 2014, 2022; Fralick and Riding, 2015). The giant hybrid domes rimming the carbonate portion of the platform were far enough removed from the oxygen producing central lagoon that Fe^{2+} levels were higher, favouring aragonite precipitation. However, the position of the chemocline offshore from them varied depending on biologic productivity; small variations in relative sealevel; and seasonally changing current activity, e.g. storm events and upwelling events (Riding et al., 2014, 2022; Fralick and Riding, 2015).

These effects of changing water chemistry are recorded in sample SR-20 (Fig. 11). The Sr content decreases and the Fe increases upward through the basal cusped fenestral microbialite toward the dark Fe-Mn-Si-rich layer, consistent with increased alteration of the aragonite (with Sr preferentially in its lattice) to ferroan dolomite (with Fe preferentially in its lattice) (e.g. Brand and Veizer, 1980; Veizer et al., 1989). This is accompanied by a decrease in negative Ce anomalies to a point where they only exist sporadically. The overlying dark alteration layer represents replacement of aragonite by ferroan dolomite and silica, and precipitation of iron hydroxide (e.g. Fig. 2E and caption; also, Kurucz and Fralick, 2018). Above this layer strontium levels are low, but Mn and Fe concentrations in the calcite are approximately five times greater than in the lower layer, although they decrease upward (Fig. 10). This suggests the original presence of calcite, due to Fe and Mn fitting into the calcite lattice more readily than the aragonite lattice and the opposite for Sr.

The elevated amount of Sr and low amounts of Fe and Mn in the lower layer indicates it was aragonite, and negative Ce anomalies suggest that the chemocline, where Fe^{2+} , Mn^{2+} and Ce^{3+} were being removed from solution, was located offshore in the area of active accumulation of iron hydroxides and manganese oxides (Riding et al., 2022), which would also cause oxidation of Ce^{3+} to relatively insoluble Ce^{4+} . Overall, this would have depleted the seawater in Fe^{2+} , Mn^{2+} and Ce^{3+} , limiting the abundance of these elements in the shallow water, Ca-carbonate dominated platform area. Nonetheless, the layer of dark alteration suggests episodic, shore-ward migration of the chemocline that increased concentrations of Fe^{2+} , terminated aragonite precipitation, locally replaced aragonite on the seafloor with Fe-rich carbonate, and facilitated Fe-hydroxide precipitation. This process continued until the drawdown of Fe^{2+} content in the water was sufficient to allow Ca-carbonate precipitation to resume (see also Klein and Beukes, 1989; Sumner, 1997b; Canfield, 2005; Riding et al., 2014, 2022). The amount of Mn^{2+} and Fe^{2+} in the water continued to decrease as Ca-carbonate precipitated, and Ce delivered during the flooding event was oxidized and removed from the seawater, resulting in either no Ce anomaly, or positive Ce anomalies in the calcite.

The differences between the lithofacies are evident in Figs. 7, 8 and 9, with the originally aragonite crystal fan fabric and cusped fenestral microbialite of the site #1 giant hybrid domes plotting with relatively high Sr and Ba, low Fe and Mn and strongly negative Ce anomalies. This represents the positioning of the chemocline and its associated iron hydroxide, manganese oxide and Ce^{4+} deposits offshore from these carbonate platform rim lithofacies. In contrast, the calcite net-like fenestral microbialite has intermediate Sr, Ba, Fe and Mn, and no to positive Ce anomalies. The greater original porosity and permeability of

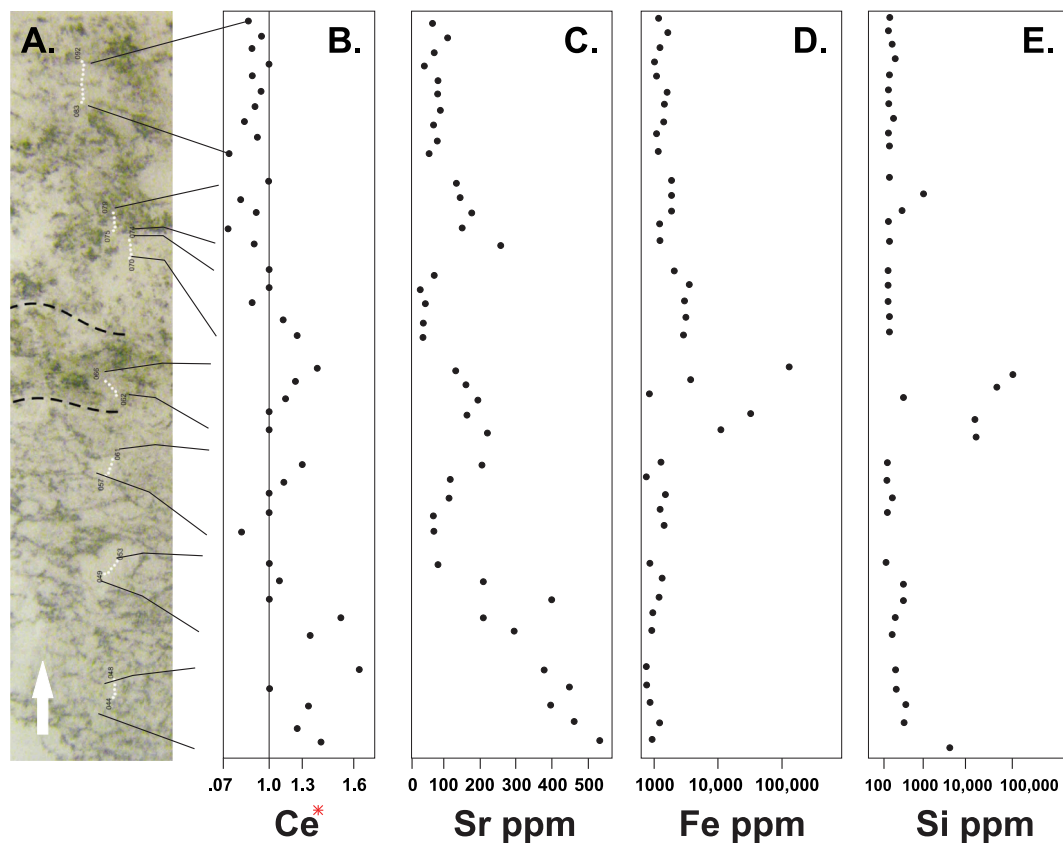


Fig. 11. Limestone sample SR-20 (Fig. 3C). (A.) This is the LA-ICP-MS line, shown in Fig. 3C and 9, along which 40 analyses were made. Sr content (C) decreases up through the lower laminae, with the negative Ce anomaly (B) also decreasing, though with more scatter. As the dark laminae, marked by the dashed lines, is approached the Sr content and the negative Ce anomaly. The Sr content decreases up through the dark lamina, whereas the negative Ce anomaly increases both increase. This layer is highly enriched in Fe (D) and Si (E) (note the logarithmic scale for these elements), with the highest Fe and Si values corresponding to a large negative Ce anomaly. The Ce anomaly in the layer above the dark laminae changes from negative to positive, and persists upward as positive to neutral. This layer has a greater Fe content in the calcite than the layer below the dark laminae, though the amount of Fe does generally decrease upwards.

the net-like fabric (e.g. Sumner, 1997a) would have allowed greater pore water flow producing a high water/rock ratio (e.g. Brand and Veizer, 1980). It is the large amount of blocky cement formed in the pores and producing the net-like fabric (Sumner, 1997a) that has intermediate Sr, Ba, Fe and Mn, and no to positive Ce anomalies. The net-like fabric in SR-16 and SR-20 have Mn/Fe ratios greater than one compared to ratios less than one in the Fans, which formed from seawater. Thus, the net-like fabric chemistry is probably that of the pore water and does not reflect that of seawater.

The net-like fenestral microbialite in the basal layer of sample SR-16 (Fig. 5) is the only layer studied at site #1 that shows significant evidence of late diagenetic mobilization and overprinting by ferroan dolomite. It exhibits a positive Eu anomaly, indicating involvement of Archean seawater and, on average, no pronounced Ce anomaly. The individual Ce anomaly data-points from this layer range from 0.65 to 1.4, with a large amount of scatter and no trend. In contrast, the fenestral microbialite above it at the base of the fans, as well as the large crystal fan fabric forming the upper half of the sample, have negative Ce anomalies. It is possible that the fluid that introduced the Mg, Fe and Mn into the basal layer caused REE fractionation that created the small-scale lateral variations in composition. However, this may have occurred with net REE subtraction from, or addition to, the layer, since the average normalized REE pattern (Fig. 5) is typical of Archean open ocean seawater (see Kamber et al., 2004, p. 386; Kamber and Webb, 2001; Van Kranendonk et al., 2003). The silicified layer above this has a slight positive Eu anomaly and slight negative Ce anomaly. It is followed upward by crystal fans with no Eu anomaly and significant negative Ce anomalies. Aside from a few thin ferroan dolomite veins that do not have

alteration halos, the layers above the basal net-like fenestral microbialite lack either visible or chemical evidence of alteration, and are similar to previously published REE patterns of Steep Rock crystal fans and cusped fenestral fabric (Fralick and Riding, 2015).

The crystal fans, which grew on the seafloor by precipitation from the overlying water (Sumner and Grotzinger, 2000, 2004), differ in chemistry from the inter-crystal cements and capping alteration surfaces, which have less Sr and Ba (Fig. 5) and more Mg, Fe, Mn, Si and Al (Figs. 4, 5, 7, 8). The upper alteration surfaces probably represent localized dolomitization and silicification due to influx of offshore seawater (Fralick and Riding, 2015; Riding et al., 2022), with siliciclastics accumulating during this interval. The cements would have formed later, from seawater that was trapped as pore water. The preservation of these discrete chemistries during sub-seafloor diagenesis requires a low water/rock ratio for diagenetic pore fluids as they are susceptible to being homogenized by localized dissolution of precursor carbonate and development of partially closed reaction zones (see Kinsman, 1969; Pingitore, 1976; Katz and Matthews, 1977; Veizer, 1977; Brand and Veizer, 1980). In general, the presence of Al in siliciclastics associated with sea-floor alteration surfaces often suggests that alteration occurred over a sufficient period of time for wind-blown clay to accumulate on an isolated platform that lacked local siliciclastic sources (Fralick et al., 2008).

These details demonstrate the dynamic nature of the water masses in this carbonate system in which aragonite precipitation dominated on the outer edge of the platform and calcite precipitated in the interior (Riding et al., 2014; Fralick and Riding, 2015; Riding et al., 2022). In addition, and superimposed on this, incursions of offshore water led to

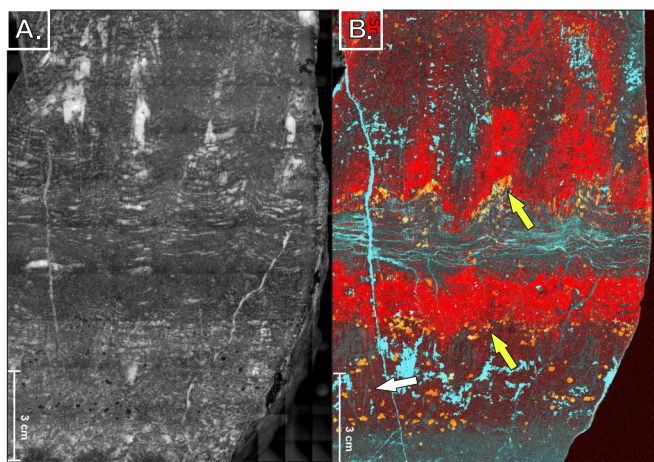


Fig. 12. (A.) Limestone sample SR-0 from Site #2. Net-like fenestral microbialite in the basal one third is overlain in the middle one third by a very dark layer of cusped fenestral microbialite that becomes lighter upwards. Crystal fans grow from the upturned edges of the cusped structures. White void-filling cement is common, especially between clusters of crystal fans. (B.) XRF scan of A with Sr in red, Mn in blue and Si in yellow. The lower net-like fenestral microbialite is divisible into two layers: the lower one with larger fenestrae has low Sr and larger amounts of Mn (and Fe and Al, not shown). The overlying lamina is richer in Sr and Si with evidence of secondary Mn mobilization and concentration in associated late-stage porosity. Faint small crystal fans are present (white arrow). There is minor Si concentration at the top of the layer (lower yellow arrow); this is overlain by a very Sr- and C-rich layer of cusped fenestral microbialite. The upper half of the cusped fenestral microbialite is chemically similar to the layer immediately below the Sr-rich portion of the layer, but contains sub-horizontal Mn-rich veins instead of irregular void fills. High-standing areas at the edges of cusped laminae, where they meet, have concentrations of Si at the base of clumps of crystal fans (upper yellow arrow). The fans have abundant Sr, but the intervening white blocky cements do not.

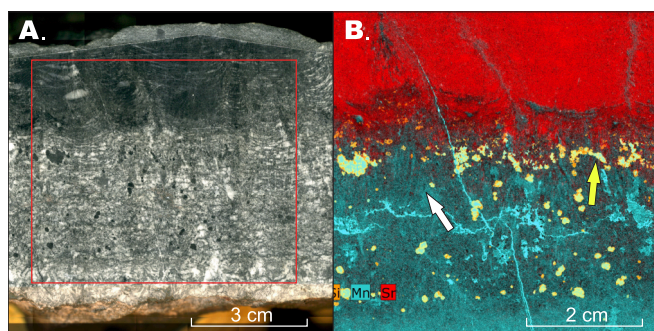


Fig. 13. (A.) Limestone sample 8 from Site #2. Net-like fenestral microbialite overlain by black, carbon-rich cusped fenestral microbialite. (B.) XRF false colour image of limestone sample 8 (red square). The blue Mn-rich (and Fe and Al not shown here) lower layer contains thin blades of radiating crystal fan fabric (white arrow) and Fe-, Mg-, and Mn-rich veins associated with irregular Mn-rich carbonate replaced areas. This is overlain by red Sr-rich cusped fenestral microbialite. The two layers are separated by yellow Si concentrations along their contact.

replacement of the surface layers of aragonite and calcite by ferroan dolomite and silica, together with precipitation of iron hydroxides in some areas.

Elevated amounts of Sr suggest an aragonite precursor to the calcite in the crystal fan (Figs. 4, 5, 6, 7) and cusped fenestral fabrics (Figs. 7, 10, and 11), compared to the majority of net-like fenestral fabric, which was probably originally calcite with lower amounts of Sr (Figs. 4, 5, 7, 10, and 11). The chemical differences between these two types of microbialite may be due to net-like fenestral fabric containing

significantly more large crystals of blocky cement than the cusped fenestral fabric. Nonetheless, preservation of these distinct chemical differences in juxtaposed laminae requires that diagenetic reactions with pore waters were limited by the existence of closed to partially closed diagenetic systems (i.e., Brand and Veizer, 1980). If this had not been the case, chemical homogenization of the layers should have resulted.

Aside from the previously mentioned seafloor alteration, there is scant evidence for significant diagenetic alteration of samples from site #1. In the lowest net-like microbialite of sample SR-16, mobilization of Mg, Fe and Mn has formed areas replaced by ferroan dolomite, which also forms veins that cut the overlying layers (Fig. 5). However, there is no evidence of Mn-enrichment in the calcite adjacent to the irregular replaced areas and veins, although this is present in the samples from site #2 (Figs. 12 and 13).

5.2. Site #2

Samples of crystal fans (Fig. 12), net-like fenestral microbialite (Figs. 12 and 13), and cusped fenestral microbialite (Figs. 12 and 13) from site #2 are calcite, though large amounts of Sr in the carbon-rich large crystal fans and cusped fenestral microbialite indicate they were originally aragonite (Riding et al., 2014; Fralick and Riding, 2015). Small, needle-like crystal fans form relic structures in the net-like fenestral microbialite fabric (white arrows, Figs. 12 and 13). Some needle-like crystals and portions of these crystals have higher Sr content, especially closer to overlying Sr-rich cusped fenestral microbialite layers. Higher concentrations of Mn occur between and within some crystals. The presence of ferroan dolomite veins in these areas, with Mn replacement extending from the veins, calls into question an original Mn-rich mineralogy for these crystal fans. The matrix surrounding the crystals in the fenestral fabric of sample SR-0 (Fig. 12, white arrow) has an intermediate amount of Sr, with Mn enrichment. The Sr-rich cusped fenestral microbialite layer in the middle of the sample (Fig. 12) is transitional to an area of Mn-enrichment associated with stratiform Mn-Fe-Mg veins. The ferroan dolomite veins associated with Mn enriched carbonate halos reflect the mobility of these elements. Mobilization likely occurred after significant lithification, as the vertical veins are not compressed. Dark zones at the base of layers of large crystal fans and cusped fenestral microbialite, have abundant quartz, ferroan dolomite and, locally, iron oxides. These have been interpreted as alteration/bounding surfaces (Kurucz and Fralick, 2018) developed during movement of offshore water onto the margin of the carbonate platform (Fralick and Riding, 2015; Kurucz and Fralick, 2018; Riding et al., 2022).

The presence of crystal fans in the net-like fenestral fabric, which are only visible using XRF elemental scans, poses a compositional question. The white blocky cement that forms more than 50 percent of these layers overprints the fans, which must extend through portions of the cement. Thus, was the net-like fenestral fabric contemporaneous with primary fans that grew in this sediment, and cement later overprinted the fans, or was the net-like structure produced later by alteration product of a layer of small crystal fans? The former seems much more likely, but the latter, especially in combination with the former, remains possible. Fans such as these have been interpreted as originally either aragonite (Martin et al., 1980; Sumner and Grotzinger, 1996; 2000) or gypsum (Bertrand-Sarfati, 1976; Walter, 1983; Gandin et al., 2005; Gandin and Wright, 2007), with current views tending to favour aragonite (Sumner, 2004; Sumner and Grotzinger, 2004; Fralick and Riding, 2015; Kurucz and Fralick, 2018). Thus, these areas could be expected have a high Sr content, but they do not (Figs. 12 and 13). Sr may have been replaced in the carbonate structure by Mn during or after the transformation of aragonite to calcite by flooding with Mn-rich fluid, as observed in the alteration halos around veins that overprint entire layers (Figs. 12 and 13). This would also imply that REEs in the calcite lattice could be susceptible to replacement. Planavsky et al. (2010) recorded no Ce anomalies in samples from this site; a possible result of element mobility

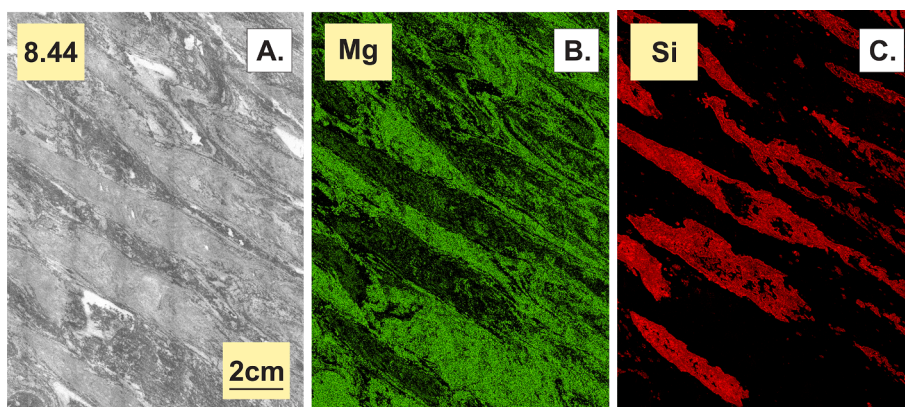


Fig. 14. (A.) Ferroan dolomite sample 8-44 (Fig. 3B) from Site #1. (B.) XRF false colour image of sample 8-44. The Mg (B), representing ferroan dolomite, concentrates in the interdigitate areas, although some laminae in the columnar stromatolites and bridging laminae across the interdigitate depressions are also Mg-rich. Quartz (C) replacement is concentrated in the stromatolite columns.

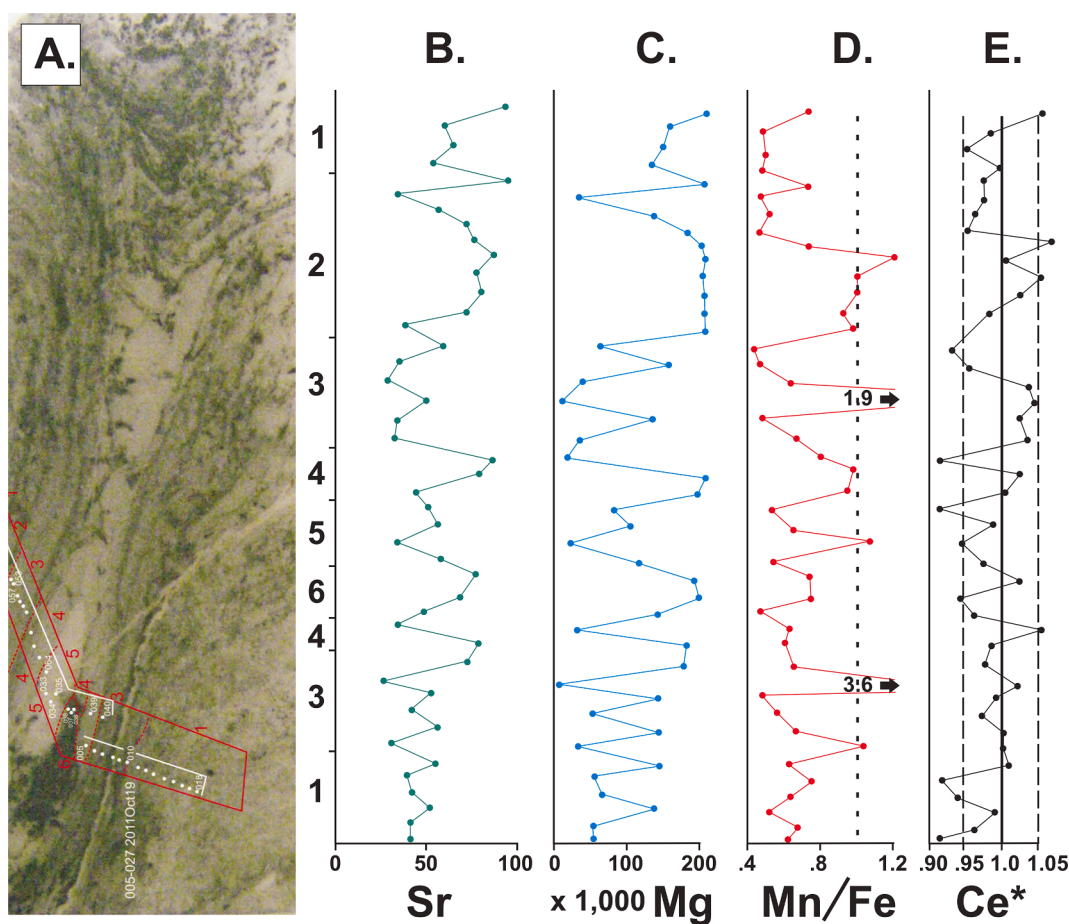


Fig. 15. A. Thin section from ferroan dolomite sample 8-44 (Fig. 3B, 14) showing lines along which LA-ICP-MS analyses were obtained across the center to edge of a narrow columnar stromatolite, the intervening white blocky cement, and the edge to center of the adjacent stromatolite. Areas 1, 3, 4 and 6 on the lower portion of the graphs are points in the stromatolite on the right. Area 5 is the interdigitate blocky cement, and areas 4-71 forming the top half on the graphs are the layers in the stromatolite on the left. Areas 1 and 3 on the right and areas 1, 2 and 3 on the left are composed of the same laminae, but the patterns for Sr (B), Mg (C), and Mn/Fe (D) are not similar. There is a large amount of variability in the patterns. Even so, with increased dolomitization (more Mg (C)) the amount of Sr (A) and the Mn/Fe ratio (D) both increase. There is no significant difference in the Sr and Mg concentrations or in the Mn/Fe ratios between the centers and edges of stromatolites and the white blocky cement between the stromatolites. Most Ce* values (E) are in the area between 0.95 and 1.05, which is within error limits of 1.0 and cannot be used to infer anomalies (Planavsky et al., 2010). However, there is a difference in the number of points below 1.0 (60 % with seven having significant positive Ce anomalies) compared to those above 1.0 (30 % with only one having a significant negative Ce anomaly). Ce anomaly ($Ce^* = Pr / (0.5Ce + 0.5Nd)$).

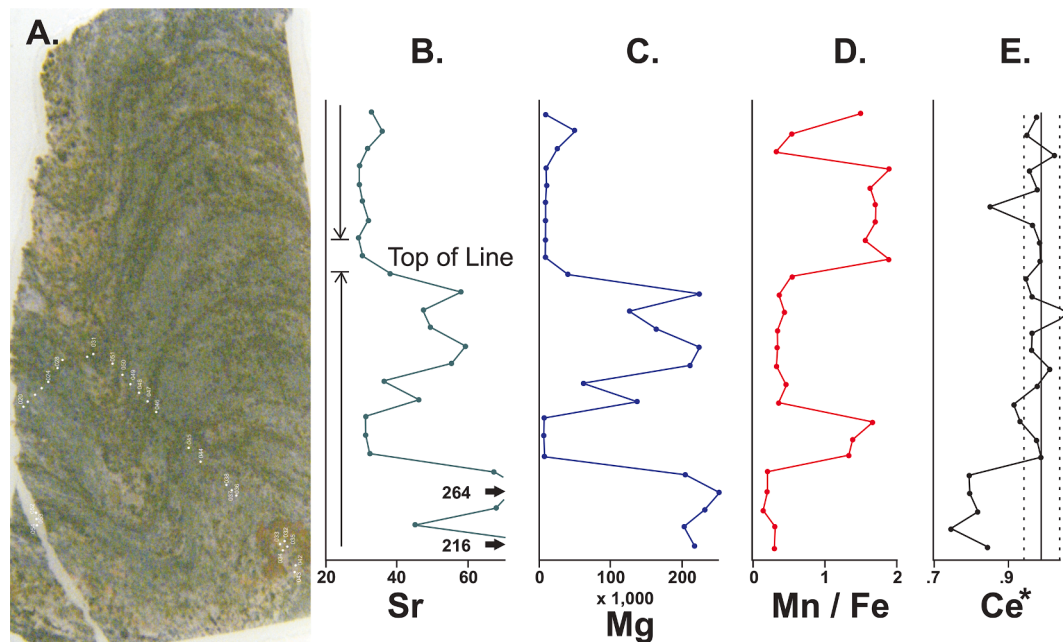


Fig. 16. (A.) LA-ICP-MS analyses along lines on of this thin section from sample 8–43 (Fig. 3A), Site #3. (B.) Greater amounts of Sr (B) correspond to areas enriched in Mg (C) (ferroan dolomite), whereas, those with very low amounts of Mg are calcite. The calcite has Mn/Fe ratios (D) above one and low amounts of Sr, whereas the ferroan dolomite has Mn/Fe ratios less than one and greater amounts of Sr. The ferroan dolomite forming the bottom five points of the line contain positive Ce anomalies (E). The remaining sample sites mostly lack discernible Ce anomalies, although the majority of the points, 88 %, are below 1, indicating general Ce enrichment. Ce anomaly ($Ce^* = Pr / (0.5Ce + 0.5Nd)$).

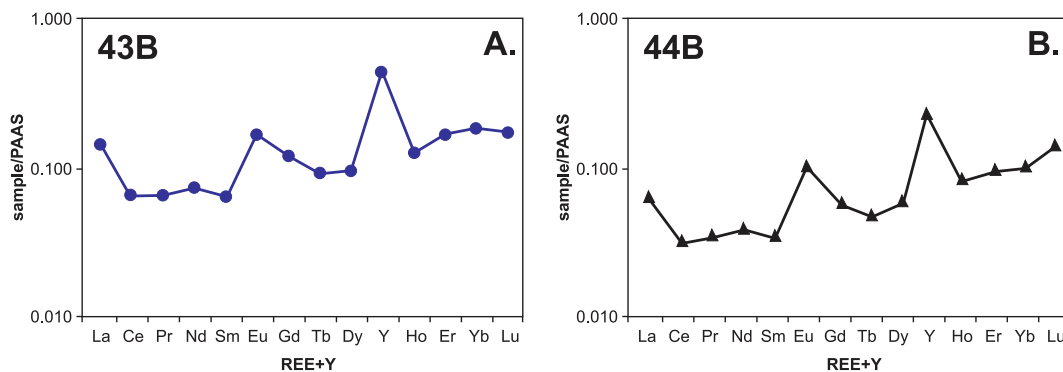


Fig. 17. Average REE patterns derived from the LA-ICP-MS data for samples 8–43 (A) and 8–44 (B) from Site #3. The average values for these primarily ferroan dolomite samples have no Ce anomalies and positive Eu and Y anomalies. This is similar to REE patterns for oxide facies iron formation that was precipitating offshore from the carbonate platform (Fig. 27 in Fralick and Riding, 2015).

in these limestones, which appear pristine in hand sample.

5.3. Site #3

The ferroan dolomite samples from site #3 include narrow columnar stromatolites from a 25 cm thick layer that is in contact with limestones on both sides and may be laterally continuous for at least 0.5 km, the distance between where samples 8–43 and 8–44 were collected. Thin ferroan dolomite laminae accentuate layering in the limestones that form the basal units of the Mosher Carbonate. They commonly have sharp upper contacts and jagged lower contacts and, in places, plugs of ferroan dolomitized layer tops were displaced upwards by soft-sediment fluid escape (Fig. 2E), suggesting dolomitization of the calcite by influxes of offshore seawater prior to lithification (Fralick and Riding, 2015). Whether the thicker layer of ferroan dolomite that was sampled represents a replacement reaction or direct precipitation from seawater is difficult to ascertain. Its $\delta^{13}C$ value is consistent with Archean seawater (Fig. 22 in Fralick and Riding, 2015). However, the Sr isotope

values have been reset (Satkoski et al., 2017). In this thicker layer preferential silicification of areas in the digitate stromatolites, and dolomitization of individual laminae in some columns (Figs. 14, 15, and 16) indicate a complex diagenetic history. Seafloor ferroan dolomitization driven by incursions of offshore seawater (Fralick and Riding, 2015; Riding et al., 2022) and syndepositional silicification of the stromatolites due to bacteria serving as nucleation templates (e.g., Beveridge, 1989; Schultze-Lam et al., 1992; Urrutia and Beveridge, 1993; Schultze-Lam et al., 1995), are distinct possibilities. The average REE patterns for samples 8–43 and 8–44 (Fig. 17) share more characteristics, i.e. low slope and significant positive Eu anomaly, with the offshore deposited magnetite and chert (Fig. 27 in Fralick and Riding, 2015) than the carbonate (Fig. 5, and Fig. 26 in Fralick and Riding, 2015). However, the LA-ICP-MS analyses of sample 8–44 depict significant mm-scale variation (Fig. 15). Concentrations of Mg and Sr are positively correlated. This does not appear to be caused by Si acting as a dilutant, as its concentration is reasonably consistent along the line of analysis. Low Mg concentrations may be due to incomplete dolomitization of calcite, but

this should also result in larger concentrations of Sr, as the surrounding limestones contain ~300 ppm Sr, compared to <50 ppm in the analyzed spots with lower Mg concentrations. This would require the original calcite to have lost Sr during conversion to ferroan dolomite by influx of open ocean seawater (e.g. Kinsman, 1969; Brand and Veizer, 1980) and to then lose even more Sr during later partial dedolomitization. This trend is even more pronounced in sample 8–43 where low amounts of Mg (Fig. 16) are due to the presence of calcite, but these areas also have very low amounts of Sr. Again, this suggests dolomitization followed by diagenetic dedolomitization causing a two-step Sr loss. The majority of analyzed spots do not have distinct cerium anomalies, although there are significantly more values below 1 than above 1. Eight significant positive Ce anomalies occur in the ferroan dolomite of Sample 8–43 (Fig. 16), and five of these are associated with the greatest concentrations of Sr, up to 264 ppm, which is similar to the surrounding limestone. This is consistent with these being the least altered of all the spots analyzed, therefore preserving some chemical characteristics of the original mineralogy. However, caution must be exercised as investigation of a partially dolomitized Devonian reef complex concluded that the REEs had been modified during the replacement process (Nothdurft et al., 2004). For this to be the case the dolomitizing fluids must be significantly different from those from which the calcite or aragonite precipitated (Banner et al., 1988).

The further depletion of Sr in the calcite, relative to values in the ferroan dolomite, indicates an additional period of alteration following dolomitization. This dedolomitization fluid would have been rich in Ca and very poor in Mg, Fe and Mn and probably developed during partial dissolution of the large volume of surrounding limestone. It is not known whether the REEs would have fractionated during the dissolution and/or

replacement processes that led to dedolomitization, although in Devonian dolomites they did (Nothdurft et al., 2004).

Overall, these detailed analyses show that both synsedimentary and later stage diagenetic alteration can overprint and remove evidence of negative Ce anomalies in Mid-Archean shallow-marine carbonates, even in fabrics that superficially appear relatively well-preserved, and this alteration can be very localized. These conclusions are summarized in Fig. 18.

5.4. Summary

The crystal fan fabric represents precipitation sites that were protruding, if only slightly (Sumner and Grotzinger, 2000), into the overlying seawater and precipitating from it. The cusate fenestral and net-like fabrics are interpreted as microbial and are thought to have also formed in contact with seawater (Sumner, 1997a, Sumner and Grotzinger, 2000), as did the stromatolites. They should therefore record its REE composition (e.g. Webb and Kamber, 2000). The differences in geochemistry among these various carbonate deposits show that changes in the composition of the water was occurring through space and/or time. The most likely paragenesis sequence of the samples can be summarized as follows:

- (1) A gradient in the geochemistry of the seawater existed between that which was precipitating calcite in the central lagoon and that which was depositing low-Mn iron formation (Huston, 1956) far offshore (Riding et al., 2014, 2022; Fralick and Riding, 2015). Closer to the carbonate portion of the platform the Mn content of the iron formation became significant (Huston, 1956). This would

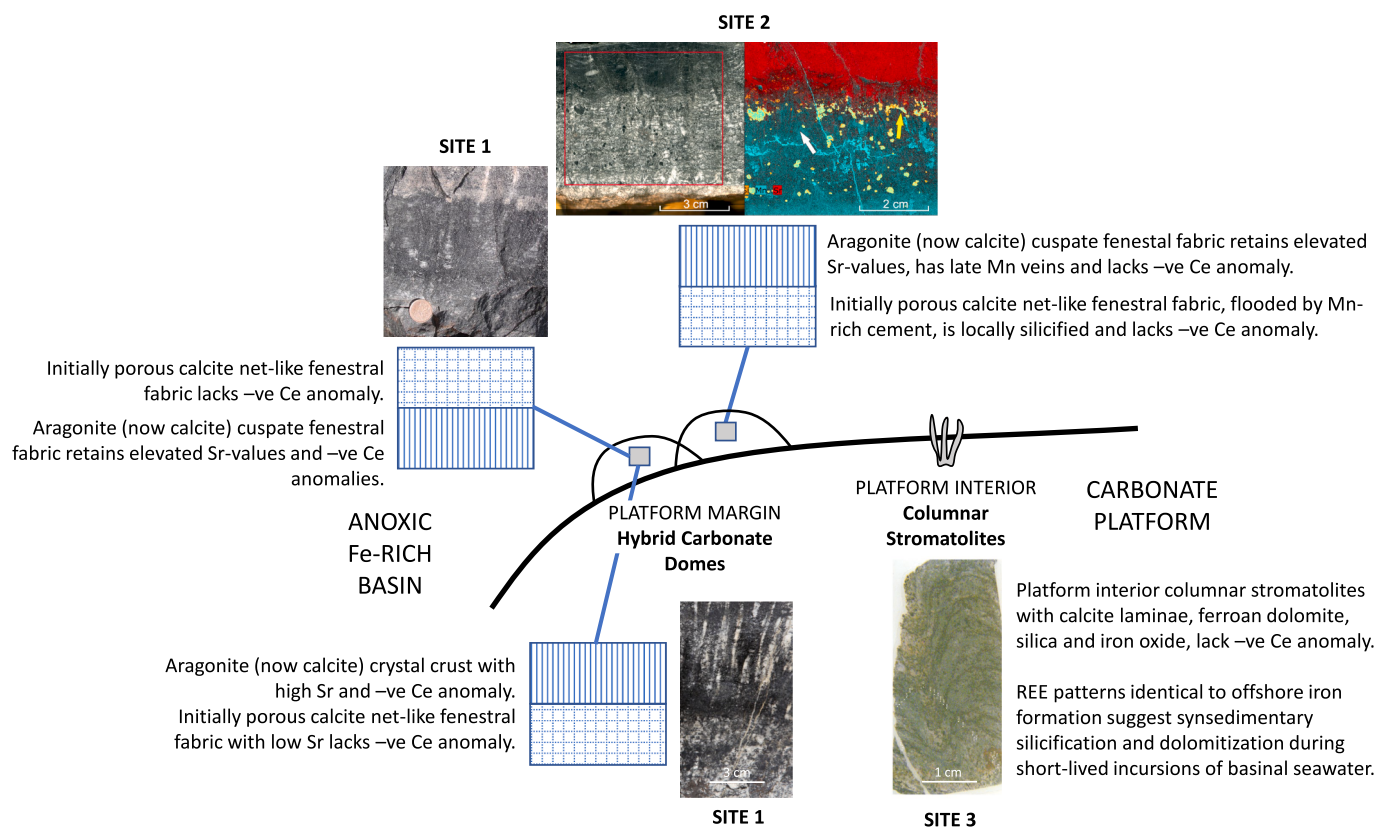


Fig. 18. Summary interpretation: Detailed analyses indicate that synsedimentary and late diagenetic alteration can locally readily overprint and remove evidence of negative Ce anomalies in these Mid-Archean shallow-marine carbonates that otherwise retain relatively well-preserved fabrics. In platform margin giant hybrid carbonate domes at Site #1 negative Ce anomalies were retained by originally aragonite seafloor crystal fans and cusate fenestral fabric. However, the highly porous net-like fenestral fabrics have been overwhelmed by cements that lack Ce anomalies. Closer to recognized alteration zones at Site #2 the negative Ce anomalies appear to have been removed by late diagenetic fluids rich in Mn and Si. At Site #3, platform interior columnar stromatolites lacking negative Ce anomalies, have, in places, been silicified and dolomitized, probably by offshore seawater during short-term flooding of the platform (Fralick and Riding, 2015).

- be an area where Ce^{4+} was also precipitating. Moving onto the carbonate portion of the oceanic platform, (i) in the outer region Fe^{2+} in solution would have inhibited calcite precipitation leading to the dominance of aragonite (Herzog et al., 1989; Katz et al., 1993), (ii) with decreasing Fe^{2+} concentrations in the central lagoon calcite became the dominant phase (Riding et al., 2014, 2022).
- (2) The giant hybrid carbonate domes along the rim of the carbonate platform (Fralick and Riding, 2015) served to inhibit water movement. However, small changes in sealevel due to storms and/or increased subsidence rate, and variable biologic productivity due to changing nutrient supply, and/or alterations in the size of the photic zone on the carbonate platform, probably allowed the chemocline to periodically move into the central lagoon. This could lead to penecontemporaneous replacement of the surficial Ca-carbonate by ferroan dolomite and chert (Fralick and Riding, 2015; Kurucz and Fralick, 2018; Riding et al., 2022).
 - (3) Burial cements that subsequently formed in the pore spaces have different geochemical attributes than the original precipitates (e. g. Fig. 24 in Fralick and Riding, 2015; Figs. 6, 7, 8). This did not affect the blades of the crystal fans and cusped fenestral fabric, whereas the net-like fabric, due to its higher porosity, was greatly affected, with the result that most of these layers consist of cement.
 - (4) Pore waters would have been dominated by Ca^{2+} and HCO_3^- . This led to dedolomitization reactions that transformed some of the ferroan dolomite laminae back to calcite.
 - (5) An infusion of Mn-bearing fluids was associated with the development of areas of vertical oxidation that extended down from the overlying iron formation. This resulted in development of Mn-Fe-Mg carbonate veins, void fills and flooding of areas adjacent to these alteration zones. This event probably altered the REE compositions of affected layers, similar to dolomitization in the Canning Basin (Nothdurft et al., 2004).

6. Conclusions

- (1) LA-ICP-MS point analyses resulted in REE patterns that are very similar to those produced by whole rock ICP-MS (Riding et al., 2014; Fralick and Riding, 2015).
- (2) Significant negative Ce anomalies in 70 of the LA-ICP-MS analyses indicate that those samples precipitated from fluids that had reacted with free oxygen. The layers with negative Ce anomalies predominantly consist of crystal fan fabric and cusped fenestral fabric that formed on the seafloor of the carbonate platform. The cusped fenestral fabric with negative Ce anomalies has less blocky cement than the net-like fenestral fabric that lack negative Ce anomalies. It is possible that the blocky cement formed from diagenetic fluids that did not have negative Ce anomalies and that the dominance of this cement in the net-like fabric determines its REE patterns.
- (3) Higher amounts of Sr indicate less carbonate alteration, as previously shown (Brand and Veizer, 1980; Veizer et al., 1989), and negative Ce anomalies are positively correlated with greater Sr content.
- (4) Millimetre-scale differences in calcite chemical composition indicate that significant diagenetic homogenization has not occurred in most of the layers analyzed.
- (5) When subjected to XRF scanning, some samples that otherwise appear pristine reveal chemical alteration extending into the calcite from thin ferroan dolomite veins. In places this alteration was sufficient to alter entire layers. The field area in which this alteration occurs is the location of samples collected by a previous study (Planavsky et al., 2010) that did not have Ce anomalies.
- (6) Some calcite columnar stromatolites were replaced by ferroan dolomite and silica, probably during incursion of open marine

water into the platform interior (Fralick and Riding, 2015; Riding et al., 2022). REE patterns of the ferroan dolomite (Fig. 16) are similar to those of magnetite and siderite deposited offshore from the carbonate (fig. 27D, F in Fralick and Riding, 2015).

- (7) Modification of REE patterns in calcite by dolomitizing fluids was also noted in Devonian dolomites by Nothdurft et al. (2004). Sr was also lost during dolomitization. A few points in sample 8–43 have elevated Sr concentration. In two cases these are similar to those of the surrounding limestone, indicating the lowest amounts of chemical alteration in the dolomite. These are also the only ferroan dolomite samples with very significant positive Ce anomalies. These observations support the view that free oxygen was being photosynthetically produced by cyanobacterial communities in or near these stromatolites. There are calcite laminae in the ferroan dolomite stromatolites sampled. However, their Sr concentrations are depleted compared with the ferroan dolomites, probably due to further Sr loss during dedolomitization.
- (8) This research highlights the ability of microanalytical tools, such as XRF scanning, LA-ICP-MS, and SEM-EDX, to provide critical information regarding micro-scale chemical changes in the composition of individual calcite and dolomite layers. Together with detailed fieldwork, these data can be related to the effects of both dynamic depositional processes that changed through time, and to diagenetic alteration of the primary sediment. Information such as this is essential for the reliable interpretation of geochemical data obtained from sedimentary and metasedimentary rocks.

Declaration of competing interest

The authors declare that they have no known competing financial interests or personal relationships that could have appeared to influence the work reported in this paper.

Data availability

Data will be made available on request.

Acknowledgements

We are grateful to Andreas Klügel (University of Bremen) for support during LA-ICP-MS analyses. We greatly appreciate the comments of Fulvio Franchi and two anonymous reviewers that greatly improved the manuscript and the tireless editorial advice of Frances Westall. Data processing was assisted by Tim McIntyre and Sophie Kurucz. Drafting was by Jordan Heroux. This research was supported by a Canadian Natural Science and Engineering Discovery Grant to P. F. and the European Union's Horizon 2020 research and innovation program (grant agreement no. 716515) grant to S. V. L.

References

- Afroz, M., Fralick, P.W., Lalonde, S.V., 2023. Sedimentology and geochemistry of basinal lithofacies in the Mesoproterozoic (2.93 Ga) Red Lake carbonate platform, northwest Ontario, Canada. *Precambrian Research* 388 <https://doi.org/10.1016/j.precamres.2023.106996>.
- Alibert, C., McCulloch, M.T., 1993. Rare earth element and neodymium isotopic composition of the banded iron formations and associated shales from Hamersley, western Australia. *Geochim. Cosmochim. Acta* 57, 187–204.
- Banner, J.L., Hanson, G.N., Myers, W.J., 1988. Rare earth element and Nd isotopic variations in regionally extensive dolomites from the Burlington-Keokuk Formation (Mississippian): Implications for REE mobility during carbonate diagenesis. *J. Sediment. Petrol.* 58, 415–432.
- Barrett, T.J., Fralick, P.W., Jarvis, I., 1988. Rare-earth-element geochemistry of some iron formations north of Lake Superior, Ontario. *Can. J. Earth Sci.* 25, 570–580.
- Bathurst, R.G.C., 1975. Carbonate Sediments and their Diagenesis. In: *Developments in Sedimentology* 12, 2nd ed. Elsevier, Amsterdam, p. 658.
- Bau, M., Dulski, P., 1996. Distribution of yttrium and rare-earth elements in the Penge and Kuruman iron-formations, Transvaal Supergroup, South Africa. *Precambrian Research* 79, 37–55.

- Bau, M., Moller, P., 1993. Rare earth element systematics of the chemically precipitated component of Early Precambrian iron formations and the evolution of the terrestrial atmosphere-hydrosphere-lithosphere system. *Geochim. Cosmochim. Acta* 57, 2239–2249.
- Bertrand-Sarfati, J., 1976. Pseudomorphoses de gypse en rosettes dans un calcaire cryptalga-laminaire du Précambrien inférieur (Système du Transvaal, Afrique du Sud). *Bull. Soc. Géol. France* 3, 99–102.
- Beveridge, T.J., 1989. Role of cellular design in bacterial accumulation and mineralization. *Annu. Rev. Microbiol.* 43, 147–171.
- Bolhar, R., Kamber, B.S., Moorbath, S., Fedo, C.M., Whitehouse, M., 2004. Characterization of early Archaean chemical sediments by trace element signatures. *Earth Planet. Sci. Lett.* 222, 43–60.
- Bolhar, R., Van Kranendonk, M.J., 2007. A non-marine depositional setting for the northern Fortescue Group, Pilbara Craton, inferred from trace element geochemistry of stromatolitic carbonates. *Precamb. Res.* 155, 229–250.
- Bolhar, R., Van Kranendonk, M.J., Kamber, B.S., 2005. A trace element study of siderite-jasper banded iron formation in the 3.45 Ga Warrawoona Group, Pilbara Craton – formation from hydrothermal fluids and shallow water. *Precamb. Res.* 137, 93–114.
- Brand, U., Veizer, J., 1980. Chemical diagenesis of a multi-component carbonate system – 1: Trace elements. *J. Sediment. Petrol.* 50, 1219–1236.
- Canfield, D.E., 2005. The early history of atmospheric oxygen: homage to Robert M. Garrels. *Ann. Rev. Earth Planet. Sci.* 33, 1–36.
- Danielson, A., Moller, P., Dulski, P., 1992. The europium anomalies in banded iron formations and the thermal history of the oceanic crust. *Chem. Geol.* 97, 89–100.
- Davis, D.W., Jackson, M.C., 1988. Geochronology of the Lumby Lake greenstone belt: a 3 Ga complex within the Wabigoon subprovince, northwest Ontario. *Geol. Soc. Am. Bull.* 100, 818–824.
- Derry, L.A., Jacobsen, S.B., 1990. The chemical evolution of Precambrian seawater: evidence from REEs in banded iron formation. *Geochim. Cosmochim. Acta* 54, 2965–2977.
- Dietzel, M., Gussone, N., Eisenhauer, A., 2004. Co-precipitation of Sr^{2+} and Ba^{2+} with aragonite by membrane diffusion of CO_2 between 10 and 50 °C. *Chem. Geol.* 203, 139–151.
- Emerson, S., Hedges, J., 2004. In: Elderfield, H. (Ed.), *The oceans and marine geochemistry*. Treatise Geochem. 6, 293–319.
- Fralick P.W., Hollings, P., King, D., 2008. Stratigraphy, geochemistry and depositional environments of Mesoarchean sedimentary units in western Superior Province: implications for generation of early crust. In: K.C. Condie, V. Pease (Eds.), *When did Plate Tectonics Begin on Planet Earth*. Geological Society of America Special Paper 440, 77–96.
- Fralick, P.W., Riding, R., 2015. Steep Rock Lake: Sedimentology and geochemistry of an Archean carbonate platform. *Earth Sci. Rev.* 151, 132–175.
- Franchi, F., 2018. Petrographic and geochemical characterization of the Lower Transvaal Supergroup dolostones (Kanye Basin, Botswana). *Precamb. Res.* 310, 93–113.
- Gandin, A., Wright, D.T., 2007. Evidence of vanished evaporites in Neoproterozoic carbonates of South Africa. In: B.C. Schreiber, S. Lugli, M. Babel (Eds.), *Evaporites through Space and Time*. Geological Society Special Publication 285, 285–308.
- Gandin, A., Wright, D.T., Melezhik, V., 2005. Vanished evaporites and carbonate formation in the Neoproterozoic Kogelbeen and Gamohaan formations of the Campbellrand Subgroup, South Africa. *J. Afr. Earth Sci.* 41, 1–23.
- Herzog, R.E., Shi, Q., Patil, J.N., Katz, J.L., 1989. Magnetic water treatment: the effect of iron on calcium carbonate nucleation and growth. *Langmuir* 5, 861–867.
- Hollings, P., Wyman, D., 1999. Trace element and Sm-Nd systematics of volcanic and intrusive rocks from the Lumby Lake Greenstone belt, Superior Province: evidence for Archean plume-arc interaction. *Lithos* 46, 189–213.
- Hollings, P., Wyman, D., Kerrich, R., 1999. Komatiite-basalt-rhyolite volcanic associations in Northern Superior Province greenstone belts: significance of plume-arc interaction in the generation of the proto-continental Superior Province. *Lithos* 46, 137–161.
- Huston, W.J., 1956. The Steep Rock manganeseiferous footwall paint. MSc. Thesis, Queens University, Kingston, Ontario, p. 76.
- James, N.P., Jones, B., 2016. Part III Carbonate diagenesis: an overview. In: N.P. James and B. Jones, *Origin of Carbonate Sedimentary Rocks*. Wiley, Oxford, U.K., 273–426.
- James, N.P., Choquette, P.W., 1983a. Diagenesis 5. limestones: introduction. *Geosci. Can.* 10, 159–161.
- James, N.P., Choquette, P.W., 1983b. Diagenesis 6. limestones — the sea floor diagenetic environment. *Geosci. Can.* 10, 162–179.
- James, N.P., Choquette, P.W., 1984. Diagenesis 9. limestones - the meteoric diagenetic environment. *Geosci. Can.* 11, 161–194.
- Jochum, K.P., Nohl, U., Herwig, K., Lammel, E., Stoll, B., Hofmann, A.W., 2005. GeoReM: a new geochemical database for reference materials and isotopic standards. *Geostand. Geoanal. Res.* 29, 333–338.
- Jolliffe, A.W., 1955. Geology and iron ores of Steep Rock Lake. *Econ. Geol.* 50, 373–398.
- Kamber, B.S., Webb, G.E., 2001. Geochemistry of late Archean microbial carbonate: implications for ocean chemistry and continental erosion history. *Geochim. Cosmochim. Acta* 65, 2509–2525.
- Kamber, B.S., Bolhar, R., Webb, G.E., 2004. Geochemistry of late Archean stromatolites from Zimbabwe: evidence for microbial life in restricted epicontinental seas. *Precamb. Res.* 132, 379–399.
- Katz, A., Matthews, A., 1977. The dolomitization of CaCO_3 : an experimental study at 252–295 °C. *Geochim. Cosmochim. Acta* 41, 297–308.
- Katz, J.L., Reick, M.R., Herzog, R.E., Parsiegla, K.L., 1993. Calcite growth inhibition by iron. *Langmuir* 9, 1423–1430.
- Katz, A., Sass, E., Starinsky, A., Holland, H.D., 1972. Strontium behavior in the aragonite-calcite transformation: an experimental study at 40–98 °C. *Geochim. Cosmochim. Acta* 36, 481–496.
- Kimberley, M.M., Sorbara, J.P., 1976. Post-Archean Weathering of Steep Rock Group Iron Formation. University of Toronto Press, Toronto.
- Kinsman, D.J.J., 1969. Interpretation of Sr^{2+} concentrations in carbonate minerals and rocks. *J. Sediment. Petrol.* 49, 937–944.
- Kinsman, D.J.J., Holland, H.D., 1969. The co-precipitation of cations with CaCO_3 , IV. The co-precipitation of Sr^{2+} with aragonite between 16° and 96°. *Geochim. Cosmochim. Acta* 33, 1–17.
- Klein, C., Beukes, N.J., 1989. Geochemistry and sedimentology of a facies transition from limestone to iron-formation deposition in the early Proterozoic Transvaal Supergroup, South Africa. *Econ. Geol.* 84, 1733–1774.
- Kurucz, S., Fralick, P.W., 2018. Internal fabric of giant domes in the Mesoarchean Steep Rock carbonate platform, Superior Province, Canada. *Can. J. Earth Sci.* 55, 343–355.
- Lawrence, M.G., Greig, A., Collerson, K.D., Kamber, B.S., 2006. Rare earth element and yttrium variability in south east Queensland waterways. *Aquat. Geochem.* 12, 39–72, 10.107/s10498-005-4471-8.
- Machado, A.B., 1987. On the origin and age of the Steep Rock buckshot, Ontario, Canada. *Chem. Geol.* 60, 337–349.
- Martin, A., Nisbet, E.C., Bickle, M.J., 1980. Archean stromatolites of the Belingwe Greenstone Belt, Zimbabwe (Rhodesia). *Precamb. Res.* 13, 337–362.
- Mavromatis, V., Goetschl, K., Grengg, C., Konrad, F., Purgstaller, B., Dietzel, M., 2018. Barium partitioning in calcite and aragonite as a function of growth rate. *Geochim. Cosmochim. Acta* 237, 65–78.
- McIntyre, T., Fralick, P., 2017. Sedimentology and geochemistry of the 2930 Ma Red Lake-Wallace Lake carbonate platform, western Superior Province. *The Depositional Record, Canada*, 10.1002/dep2.36.
- Morse, J.W., 2004. Formation and diagenesis of carbonate sediments. In: F.T. Mackenzie ed., *Sediments, Diagenesis and Sedimentary Rocks*. Treatise Geochem. 7, 65–85.
- Nisbet, E.G., Wilks, M.E., 1989. Archean stromatolite reef at Steep Rock Lake, Atikokan, Northwestern Ontario. In: H.H.J. Geldsetzer, N.P. James, G.E. Tebbutt eds., *Reefs, Canada and Adjacent Area*. Can. Soc. Petrol. Geol. Memoir 13, 89–92.
- Northdurft, L.K., Webb, G.E., Kamber, B.S., 2004. Rare earth element geochemistry of Late Devonian reefal carbonates, Canning Basin, Western Australia: confirmation of a seawater proxy in ancient limestones. *Geochim. Cosmochim. Acta* 68, 263–283.
- Pearce, N.J.G., Perkins, W.T., Westgate, J.A., Gorton, M.P., Jackson, S.E., Neal, C.R., Chenery, S.P., 1997. A compilation of new and published major and trace element data for NIST SRM 610 and NIET SRM 612 glass reference materials. *Geostand. Newslett.* 21, 157–161.
- Pingitore Jr., N.R., 1976. Vadose and phreatic diagenesis: products and their recognition in corals. *J. Sediment. Petrol.* 46, 985–1006.
- Planavsky, N., Bekker, A., Rouxel, O.J., Kamber, B., Hofmann, A., Knudsen, A., Lyons, T. W., 2010. Rare earth element and yttrium composition of Archean and Paleoproterozoic Fe formations revisited: new perspectives on the significance and mechanisms of deposition. *Geochim. Cosmochim. Acta* 74, 6387–6405.
- Riding, R., Fralick, P., Liang, L., 2014. Identification of an Archean marine oxygen oasis. *Precamb. Res.* 251, 232–237.
- Riding, R., Liang, L., Fralick, P., 2022. Oxygen-induced chemocline precipitation between Archean Fe-rich and Fe-poor carbonate seas. *Precamb. Res.* 383 <https://doi.org/10.1016/j.precamres.2022.106902>.
- Rimstidt, J.D., Balog, A., Webb, J., 1998. Distribution of trace elements between carbonate minerals and aqueous solutions. *Geochim. Cosmochim. Acta* 62, 1851–1863.
- Satkoski, A.M., Fralick, P.W., Beard, B.L., Johnson, C.M., 2017. Initiation of modern-style plate tectonics recorded in Mesoarchean marine chemical sediments. *Geochim. Cosmochim. Acta* 209, 216–232.
- Schultze-Lam, S., Harauz, G., Beveridge, T.J., 1992. Participation of a cyanobacteria S-layer in fine-grained mineral formation. *J. Bacteriol.* 174, 7971–7981.
- Schultze-Lam, S., Ferris, F.G., Konhauser, K.O., Wiese, R.G., 1995. In situ silicification of an Icelandic hot spring microbial mat: implications for microfossil formation. *Can. J. Earth Sci.* 32, 2021–2026.
- Smyth, H.L., 1891. Structural geology of Steep Rock Lake, Ontario. *Am. J. Sci.* 42, 317–331.
- Sumner, D.Y., 1997a. Late Archean calcite-microbe interactions: two morphologically distinct microbial communities that affected calcite nucleation differently. *PALAIOS* 12, 302–318.
- Sumner, D.Y., 1997b. Carbonate precipitation and oxygen stratification in Late Archean seawater as deduced from facies and stratigraphy of the Gamohaan and Frisco formations, Transvaal Supergroup, South Africa. *Am. J. Sci.* 297, 455–487.
- Sumner, D.Y., Grotzinger, J.P., 2000. Late Archean aragonite precipitation: petrography, facies associations, and environmental significance. In: J.P. Grotzinger and N.P. James eds., *Carbonate Sedimentation and Diagenesis in the Evolving Precambrian World*. SEPM Special Publication Number 67, 123–144.
- Sumner, D.Y., Grotzinger, J.P., 1996. Were the kinetics of calcium carbonate precipitation related to oxygen concentration? *Geology* 24, 119–122.
- Sumner, D.Y., Grotzinger, J.P., 2004. Implications for Neoproterozoic ocean chemistry from primary carbonate mineralogy of the Campbellrand-Malmani platform, South Africa. *Sedimentology* 51, 1–27.
- Sumner, D.Y., 2004. Secular variation in Precambrian seawater chemistry and the timing of Precambrian aragonite seas and calcite seas (Comment, *Geology*, on-line form, p. e1).
- Taylor, S.R., McLennan, S.M., 1985. *The Continental Crust: Its Composition and Evolution*. Blackwell, Oxford, p. 312.
- Tomlinson, K.Y., Hughes, D.J., Thurston, P.C., Hall, R.P., 1999. Plume magmatism and crustal growth at 2.9 to 3.0 Ga in the Steep Rock and Lumby Lake area, western Superior Province. *Lithos* 46, 103–136.

- Tomlinson, K.Y., Davis, D.W., Stone, D., Hart, T.R., 2003. U-Pb age and Nd isotope evidence for Archean terrain development and crustal recycling in the south-central Wabigoon subprovince Canada. *Contrib. Miner. Petrol.* 144, 684–702.
- Urrutia, M.M., Beveridge, T.J., 1993. Mechanism of silicate binding to the bacterial cell wall in *Bacillus subtilis*. *J. Bacteriol.* 175, 1936–1945.
- Van Kranendonk, M.J., Webb, G.E., Kamber, B.S., 2003. New geological and trace element evidence from 3.45 Ga stromatolitic carbonates in the Pilbara Craton: support of a marine, biogenic origin and for a reducing Archean ocean. *Geobiology* 1, 91–108.
- Veizer, J., 1977. Diagenesis of pre-Quaternary carbonates as indicated by tracer studies. *J. Sediment. Petrol.* 47, 565–581.
- Veizer, J., Hoefs, J., Lowe, D.R., Thurstun, P.C., 1989. Geochemistry of Precambrian carbonates: II Archean greenstone belts and Archean seawater. *Geochim. Cosmochim. Acta* 53, 859–871.
- Walter M.R., 1983. Archean stromatolitic evidence of Earth's earliest benthos. In, ed. J. W. Schopf, *Earth's Earliest Biosphere*. Princeton University Press, Princeton, N.J., pp. 187–213.
- Webb, G.E., Kamber, B.S., 2000. Rare earth elements in Holocene reefal microbialites: a new shallow seawater proxy. *Geochim. Cosmochim. Acta* 64, 1557–1565.
- Wilks, M.E., Nisbet, E.G., 1985. Archean stromatolites from the Steep Rock Group, northwestern Ontario, Canada. *Can. J. Earth Sci.* 22, 792–799.
- Wilks, M.E., Nisbet, E.G., 1988. Stratigraphy of the Steep Rock Group, northwest Ontario: a major Archean unconformity and Archean stromatolites. *Can. J. Earth Sci.* 25, 370–391.
- Wyman, D., Hollings, P., 1998. Long-lived mantle-plume influence on an Archean protocontinent: geochemical evidence from the 3 Ga Lumby Lake greenstone belt, Ontario. *Geology* 26, 719–722.
- Zepeda, V.K., Kamber, B.S., Ghidan, O.Y.A., 2024. Direct accurate Eu anomaly analysis in very high Ba/Eu silicate samples by triple-quadrupole ICP-MS in mS/MS mass shift mode. *Chem. Geol.* 647 (2023), 121827.
- Zhang, K., Shields, G.A., 2022. Sedimentary Ce anomalies: secular change and implications for paleoenvironmental evolution. *Earth-Sci. Rev.* 229 <https://doi.org/10.1016/j.earscirev.2022.104015>.